Research on Breakage Characteristics in Side Milling of Titanium Alloy with C emented Carbide End Mill

Yanjie Du (823400327@qq.com)
Harbin University of Science and Technology https://orcid.org/0000-0002-7590-0834
Caixu Yue
Harbin University of Science and Technology
Xiaochen Li
Harbin University of Science and Technology
Xianli Liu
Harbin University of Science and Technology
Steven Y. Liang
Georgia Institute of Technology

Research Article

Keywords: Side milling, Tool damage, Fatigue damage, Cutting impact, Interval method

Posted Date: April 8th, 2021

DOI: https://doi.org/10.21203/rs.3.rs-393679/v1

Research on Breakage Characteristics in Side Milling of Titanium Alloy with Cemented Carbide End Mill

Yanjie Du[1], Caixu Yue[1*], Xiaochen Li[1], Xianli Liu[1], Steven Y.Liang[2]

[1] Key Laboratory of Advanced Manufacturing and Intelligent Technology, Ministry of Education, Harbin University of Science and Technology, Harbin 150080, China
[2] George W. Woodruff School of Mechanical Engineering, Georgia Institute of Technology, Atlanta, GA, USA
[*] yuecaixu@hrbust.edu.cn

Abstract
Aiming at the breakage of tool and low precision of the machined surface in the high-speed milling process of titanium alloy, damage mechanics is used to reveal the formation mechanism of tool fatigue breakage during the milling and determine the critical condition of tool breakage. Cutting edge chipping caused by random impact fracture during the evolution of tool damage is the main failure form of tool fatigue breakage. Based on continuous damage mechanics, fatigue crack growth theory and sliding crack energy balance equation, the crack growth law of tool material is studied under different cutting impact, and the initial damage value and critical damage value of tool material fracture based on the interval method are obtained. And the impact fracture limit conditions of the end mill edge are established including cutting parameters, material hardness, tool damage, tool wear, and cutting impact, which provide a theoretical basis for determining the cutting parameters. A titanium alloy milling experiment is carried out to define the impact damage morphology of the tool in different states after the tool is damaged. The obtained tool safety area range is verified, and the research results provide parameter optimization for the high-speed and high-efficiency milling titanium alloy process.
Keywords: Side milling, Tool damage; Fatigue damage; Cutting impact; Interval method

Declarations

Funding information

This project is supported by Projects of International Cooperation and Exchanges NSFC (Grant Number 51720105009), National Key Research and Development Project (Grant Number 2018YFB2002201), and Outstanding Youth Fund of Heilongjiang Province (Grant Number YQ2019E029)

Conflicts of interest/Competing interests

The authors declare that there is no conflict of interests regarding the publication of this article.

Availability of data and material

The datasets used or analyzed during the current study are available from the corresponding author on reasonable request.

Code availability (Not applicable)

Authors' contributions

Caixu Yue put forward the theme of the paper and established the structure of the paper; Yanjie Du established the damage model and processed the simulation data; Xiaochen Li verified the model, processed experimental data; Xianli Liu and Steven Y. Liang examined the overall structure of the paper and makes suggestions on the details of the paper.

Ethics approval

The content studied in this article belongs to the field of metal processing, does not involve humans and animals. This article strictly follows the accepted principles of ethical and professional conduct.

Consent to participate

My co-authors and I would like to opt in to In Review.

Consent for publication

I agree with the Copyright Transfer Statement.

[*] Corresponding author: Caixu YUE
E-mail: yuecaixu@hrbust.edu.cn

1 Introduction

At present, material failure is mainly to calculate damage by introducing microscopic defects. Starting from the constitutive relationship of material, material failure process undergoing damage evolution from the initial state to complete damage is studied [1]. High speed milling of titanium alloys requires cemented carbide tool to have good performance in hardness and toughness, the cemented carbide tool with finer grain can be selected to increase the impact fracture performance with the increase in hardness, the toughness will decrease. The cyclic loading, no-loading cooling, and cut-in impact on the tool in the milling process will lead to tool fatigue damage, chipping, and sticking [2]. Based on experiments, Girolamo [3] concentrated stress on micro-defects, applied cyclic loading, and analyzed experiments to modify the theory of fracture strength on the basis of microcracks.

The original microcrack in cemented carbide tool is the stress concentration area in the tool fatigue damage, and it will develop into the source of crack propagation under high stress concentration, which seriously affects the tool fatigue damage resistance. Under different cutting conditions, the tool damage will also have different changes. Firstly, there is no related experiment to prove fatigue loading of cutting tool in the milling process, and the tool breakage properties change with tool material and workpiece material, so there is not specific damage degree and damage failure criteria [4]. However, it has been explored that the crack growth rate of tool material under cyclic loading can be studied by Paris theory [5], which can further describe fatigue failure. Based on analyzing the experimental results, Gee M [6] designed fatigue experiments of cemented carbide material, and it is concluded that the fatigue life of cemented carbide is not affected by loading frequency. Llanes L [7] selected experimental indexes including fracture toughness, bending strength, and crack growth rate to research 5 kinds of cemented carbide. The results showed that the thickness of binder Co layer in YG cemented carbide had a great influence on fracture toughness. Based on the characteristics of Co layer, Chivavibul P [8] analyzed the impact damage and fatigue characteristics of various cemented carbide matrixes, including material hardness, bending strength, fracture strength, and fatigue crack propagation and many other factors. Uhlmann E [9] analyzed the influence of residual stress and coating quality on the bonding properties of the coating and cemented carbide substrates. Torres Y [10] studied crack propagation of WC-Co cemented carbide with cyclic bending fatigue experiment, which described the relationship between crack propagation rate and minimum tensile stress. Chivavibul SM [11] concluded that the fatigue life is determined by the crack propagation rate in fine grained WC-Co cemented carbide according to the fatigue experiment.

In conclusion, the fatigue of cemented carbide material is the process that tool material continuously damages and eventually leads to fracture. In the process of milling, the impact effect of milling caused by intermittent cutting, the cyclic loading, and the vibration of the end mills will lead to a large increase in the damage and accelerate the failure process. Therefore, it is urgent to study the properties of cemented carbide material and simulate the actual cyclic loading and material damage of cemented carbide tools in high speed milling of titanium alloy, so as to provide theoretical support for the failure mechanism of cemented carbide tool and impact fracture limit conditions.

Due to poor heat resistance, titanium alloy belongs to the typical difficult-to-machine material, and the milling of titanium alloy needs more complex manufacturing process. In the milling of titanium alloy, high speed cutting cause that tool breakage failure is very serious. So the end mills failure study has important significance during milling of titanium alloy.

Cemented carbide tools in the milling process will produce a lot of heat, and have good hardness and toughness in high temperature conditions,which can be widely used as a tool material in the high speed milling process. Even so, damage failure of cemented carbide tools in the high speed milling also brought serious consequences [12-14]. Based on the experiment of M11 hardened steel, Gong F [15] analyzed the mechanism of tool damage by observing and summarizing the forms of tool damage and surface morphology. Li ZJ [16] also founded that the chip deformation during cutting was carried out around the cutting edge, and the cutting force was concentrated around the main cutting edge, which resulted in greater tensile stress and greatly improved the probability of tool damage with the high speed camera on the basis of experiments. Ni XY [17] used finite element simulation to analyze the change of stress on cutting tool with time. Based on the fatigue crack model, the initiation and propagation life of the cracks at different locations are studied, and it is inferred that the fatigue fracture is caused by the coalescence of cracks. Liu B [18] found that the cutting speed and feed speed were closely related to the fracture mode and failure mechanism of the tool in intermittent turning of hardened steel. Ding CG [19] used WC-6%Co and WC-20%Co cemented carbide tools for experiments. The experimental results were further analyzed by scanning electron microscopy, and the crack propagation was successfully observed, which can conclude that the crack propagation eventually led to the tool impact damage [20]. Yan L [21] proved that the tool breakage failure also accounted for a large proportion in the actual milling process,

and the tensile stress exceeding the tool tensile strength was the fundamental factor that leads to the tool damage. Gong F [22] studied the fracture mechanism of cemented carbide tool by milling hardened steel, which further proved that the hardness of the workpiece had an effect on the tool failure, and the geometric model of tool wear and the fracture was established. Yuan Q [23] studied that when cemented carbide tools milling workpiece using large cutting parameters, the main form of tool failure was impact damage, and tool wear also lead to tool damage after a period of stable cutting. Based on the heavy duty intermittent cutting experiment of cemented carbide tool, He GH [24] expounded the formation mechanism of tool breakage, analyzed the evolution of tool failure, and obtained the tool failure condition. Based on the stress-strength theory, Wang XG [25] studied the reliability analysis of tool life, and the change of tool failure with time was described.

From the analysis of the domestic and foreign scholars study, tool damage characteristics of the research are mainly concentrated in the following aspects: tool breakage is based on the tool crack exists inside, and micro factors will extend with the milling, the impact caused by intermittent cutting and cyclic stress in the process of cutting will have an effect on tool failure, and the optimization of improving the cutting performance including the tool structure, cutting parameters.

At present, the research on tool damage is qualitative analysis mostly, and cannot be calculated quantitatively. Therefore, this paper defines three types of tool breakage including slight chipping, chipping and breakage by defining the morphology of the tool after damage in different states. Based on continuous damage mechanics, fatigue crack growth theory and sliding crack energy balance equation, the crack growth law of tool material is studied under different cutting impact, and the initial and critical damage value of tool material fracture based on the interval method are obtained. the impact fracture limit conditions of the end mill edge are established, and the tool safety area range is obtained, which provide parameter optimization milling titanium alloy process.

2 Milling force modeling

2.1 Overall milling force modeling

In essence, cutting is a process to remove excess material. The shear deformation of the material is the result of complex thermodynamic coupling between tool and workpiece. For the tool, it is necessary to overcome the friction resistance of the chip and the workpiece, and also to overcome the shear deformation force, in order to maintain the cutting process [26]. When the cutting edge is absolutely sharp, the forces acting on the chip in the first shear zone are the normal pressure F_{ns} and the shear force F_s, respectively. The force in the first shear zone is shown in Equations (1) and (2):

$$F_s = \tau_0 A_s = \frac{\tau_0 h A_e}{\sin(\phi_n)\cos\lambda_s} \tag{1}$$

$$F_{ns} = F_s \tan(\phi_n + \beta_n - \alpha_n)\cos\lambda_s \tag{2}$$

Where h is the thickness of the undeformed chip, A_e is the cutting width, β_n is the normal friction angle, and τ_0 is the shear stress at the shear exit.

According to the bond-slip model, the frictional force and normal stress on the rake face can be solved. The frictional force F_f and the positive pressure F_n in tool-chip interface can be express as:

$$\begin{cases} F_f = \int_0^{L_1} \tau_0 \, dx + \int_{L_1}^{L} \left(\frac{H_v}{0.07}\right) \tanh\left(0.07 \frac{\mu\sigma_n}{H_v}\right) dx \\ F_n = \int_0^{L} \sigma(x) dx \end{cases} \tag{3}$$

Where Hv is the Rockwell hardness of the material, L_1 is the bonding zone length of the rake face, L is the total tool-chip contact length of the rake face, μ is the friction coefficient.

$$\mu = 1.061 e^{-0.014v}\left(1 - \left(\frac{T}{T_m}\right)^{3.6}\right) \tag{4}$$

When the flank wear volume reaches a certain value, the width of the elastic contact zone remains unchanged, while the width of the plastic flow zone increases with the increase of the flank wear volume.

The friction force and extrusion force per unit length on the cutting edge of the end mill can be obtained by simplification, as shown in Equation (5):

When $VB < VB^*$,

$$\begin{cases} F_{rw}(VB) = \dfrac{\sigma_1}{3} \cdot VB \\ F_{tw}(VB) = \dfrac{\tau_1}{3} \cdot VB \end{cases} \tag{5}$$

When $VB \geq VB^*$,

$$\begin{cases} F_{rw}(VB) = \tau_1 \cdot (VB - \dfrac{2}{3} VB^*) \\ F_{tw}(VB) = \sigma_1 \cdot (VB - \dfrac{2}{3} VB^*) \end{cases} \tag{6}$$

In the oblique cutting considering the flank wear, α_n is the normal forward angle of the tool, η_c is the chip flow angle, λ_s is the inclination angle of the tool edge, F_f is the friction force on the flank face, F_n is the pressure on the rake face, F_{tw} is the tangential force on the flank face, F_{tw} the radial force on the flank face, as shown in Fig. 1.

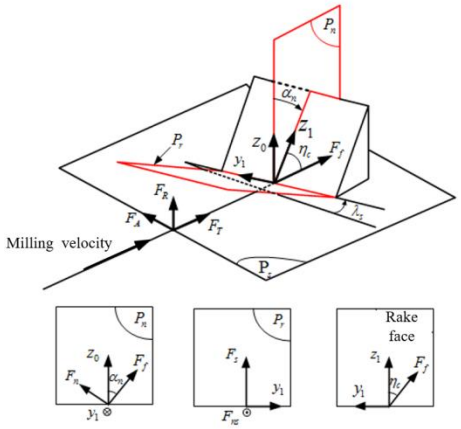

Fig. 1 The forces in the oblique cutting area

In the tool coordinate system, tangential force dF_t, radial force dF_r, and axial force dF_a can be expressed as:

$$\begin{cases} dF_r = (F_f \cos\eta_c \cos\alpha + F_n \cos\eta_c \cos(90-\alpha) + F_{rw} - F_s \cos\eta_c \cos(90-\phi_n) - F_{ns} \cos\eta_c \cos\phi_n)dz \\ dF_t = (F_f \cos\eta_c \cos(90-\alpha) - F_n \cos\eta_c \cos\alpha + F_{tw} - F_s \cos\eta_c \sin(90-\phi_n) - F_{ns} \cos\eta_c \sin\phi_n)dz \\ dF_a = (-F_f \cos(90-\eta_c) + F_n \cos(90-\eta_c) - F_s \cos(90-\eta_c) - F_{ns} \cos(90-\eta_c))dz \end{cases} \tag{7}$$

According to the geometric relationship, the correlation between undeformed chip thickness h, instantaneous contact angle θ, feed per tooth f_z and milling width A_e can be obtained [26], as shown in Equations (10) and (11):

$$h(\theta, A_e, f_z) = \begin{cases} R - \dfrac{R - Ae}{\sin\theta_1} & \theta_1 \in (\theta_{ex}, \angle XOD) \\ R - \cos\theta_2 (\sqrt{(f_z)^2 - \sec^2\theta_2 [(f_z)^2 - R^2]} - f_z) & \theta_2 \in (\angle XOD, \theta_{ex}) \end{cases} \tag{8}$$

$$\begin{cases} \theta_{ex} = \arcsin(\dfrac{f_z / 2}{R}) + 90 \\ \theta_{en} = \arcsin(\dfrac{R - Ae}{R}) \\ \angle XOD = \arctan((R - Ae) \Big/ (R\cos(\arcsin(\dfrac{R - Ae}{R})) - f_z)) \end{cases} \tag{9}$$

The end mill is discretized into m disks along the axial cutting depth, and the axial height of each disk dz can be expressed by $dl = \tan\beta dz$. According to the geometric relationship, the dz can be represented by the product of the corresponding center angle $d\theta$ and the tool radius R.

$$dz = \frac{R}{\tan\beta} d\theta \tag{10}$$

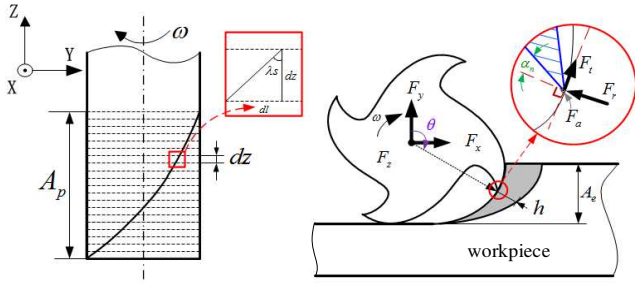

(a) Tool equidistance division (b) Magnification of single disk

Fig. 2 Discretized tool along the axis

The cutting force exerted by the disk of finite thickness is calculated in the tool coordinate system, and the force exerted by the disk in the workpiece coordinate system is obtained through the coordinate system [27]. The transformation equation is as follows:

$$\begin{bmatrix} dF_x \\ dF_y \\ dF_z \end{bmatrix} = \begin{bmatrix} -\cos\theta & -\sin\theta & 0 \\ \sin\theta & \cos\theta & 0 \\ 0 & 0 & -1 \end{bmatrix} \begin{bmatrix} dF_t \\ dF_r \\ dF_a \end{bmatrix} \tag{11}$$

In summary, in the milling process, the cutting forces in X, Y, and Z directions of the tool in the workpiece coordinate system are shown in Equation (12):

$$\begin{cases} F_x = \int_{\theta_{st}}^{\theta_{ex}} \left\{ \begin{aligned} &\left[-F_f \cos\eta_c \cos(90-\alpha_n) + F_n \cos\eta_c \cos\alpha_n - F_{tw} + F_s \cos\eta_c \sin(90-\phi_n) + F_{ns} \cos\eta_c \sin\phi_n \right] \cos\theta - \\ &\left[F_f \cos\eta_c \cos\alpha_n + F_n \cos\eta_c \cos(90-\alpha_n) + F_{rw} - F_s \cos\eta_c \cos(90-\phi_n) - F_{ns} \cos\eta_c \cos\phi_n \right] \sin\theta \end{aligned} \right\} \frac{R}{\tan\lambda s} d\theta \\ F_y = \int_{\theta_{st}}^{\theta_{ex}} \left\{ \begin{aligned} &\left[F_f \cos\eta_c \cos(90-\alpha_n) - F_n \cos\eta_c \cos\alpha_n + F_{tw} - F_s \cos\eta_c \sin(90-\phi_n) - F_{ns} \cos\eta_c \sin\phi_n \right] \sin\theta - \\ &\left[F_f \cos\eta_c \cos\alpha_n + F_n \cos\eta_c \cos(90-\alpha_n) + F_{rw} - F_s \cos\eta_c \cos(90-\phi_n) - F_{ns} \cos\eta_c \cos\phi_n \right] \cos\theta \end{aligned} \right\} \frac{R}{\tan\lambda s} d\theta \\ F_z = \int_{\theta_{st}}^{\theta_{ex}} \left[-F_f \cos(90-\eta_c) + F_n \cos(90-\eta_c) - F_s \cos(90-\eta_c) - F_{ns} \cos(90-\eta_c) \right] \frac{R}{\tan\lambda s} d\theta \end{cases} \tag{12}$$

Equation (12) is a three-dimensional cutting force prediction model based on the friction model with variable friction coefficient. The variables involved in the model are analyzed. According to the cutting parameters, tool geometric parameters, and the hardness of workpiece material, the friction characteristics in the milling of titanium alloys by cemented carbide end mill can be described, and the predicted milling force can be obtained according to the established model.

2.2 Impact force modelling

2.2.1 Normal contact force modelling

The equivalent spring damping method is usually used to transform the contact collision problem into a continuous dynamic problem, so the contact force in the machining process is calculated according to the spring damping model [28]. The equivalent spring damping model is shown in Equation (13). The specific expression of the solution of normal contact is as follows:

$$F_n = K_a \delta^e + d\dot{\delta} \tag{13}$$

Where K_a is the stiffness coefficient, δ is the deformation of the collision object, e is the index of penetration depth, d is the damping coefficient, $\dot{\delta}$ is the relative velocity of the two objects.

According to Hertz elastic contact theory, when there is no particularly prominent bulge in the shape of the contact object and the contact is made in a standard geometrical shape, the contact stiffness coefficient and stiffness index can be obtained from the inherent property parameters of the material, and then the impact force model can be obtained.

$$K_a = \sqrt{\frac{16RE_a^{\ 2}}{9}} \tag{14}$$

The specific expressions of R_3 and E_a in the above formula are as follows:

$$R_3 = \left[\frac{1}{R_1} + \frac{1}{R_2}\right]^{-1} \tag{15}$$

$$E_a = \left[\frac{1-u_1^{\ 2}}{E_{a1}} + \frac{1-u_2^{\ 2}}{E_{a2}}\right]^{-1} \tag{16}$$

Where R_1 and R_2 are respectively the effective collision radii of two collision objects at the collision point, u_1 and u_2 are respectively the Poisson's ratio of the matrix material of two collision objects, and E_{a1} and E_{a2} are respectively the three-dimensional elastic modulus of the collective material of two collision objects.

The contact force model in the collision process can be obtained from Equation (13), and solving the contact collision problem is the primary condition for using the equivalent spring damping method. For solving the damping coefficient, Equation (17) adopts the hysteretic damping model, which can be specifically expressed as:

$$D = u \cdot \delta^e \tag{17}$$

Where u is the hysteretic damping factor.

The hysteretic damping factor u can be expressed as:

$$u = \frac{3K(1-\varepsilon^2)}{4\dot{\delta}} \tag{18}$$

Where ε is the ratio of normal relative velocity of two contact objects before and after collision.

2.2.2 Tangential contact force model

When two contact objects collide, the impact force of the tool instantaneously invades the workpiece will produce normal impact force, and the relative motion between the tool and the workpiece will produce tangential friction force. Friction force is proportional to normal loading, and its direction is opposite to the relative sliding direction, and its value is not affected by the size of the contact area. Specific expression of tangential contact force is:

$$F_{s1} = \mu F_{n1} \tag{19}$$

The contact force model obtained in the local tool coordinate system is transformed into the cutting impact force model obtained in the workpiece coordinate system (XY), which is calculated as follows:

$$\begin{cases} F_{im,x} = F_{n1} \cdot \sin\varphi_f + F_{s1} \cdot \cos\varphi_f \\ F_{im,y} = F_{n1} \cdot \cos\varphi_f + F_{s1} \cdot \sin\varphi_f \end{cases} \tag{20}$$

Where φ_f is the contact angle during the collision, and its calculation is as follows:

$$\varphi_f = \pi - \arccos(1 - {ae}/{R}) \tag{21}$$

3 Damage of cemented carbide tool

The tool fatigue damage is affected by a variety of factors, which are complicated in the milling process. The tool damage can be regarded as a random situation. The milling with higher speed will produce great impact, assuming that the impact force acted on the tool is sufficient, the defects in the tool have a higher probability of breakage with more impact [29]. Since the tool damage life is related to the inherent properties of tool material, the tool fatigue damage life can be described by the physical properties of the tool.

In the process of impact fracture between cemented carbide tool and workpiece, it could be assumed that the impact phenomenon occurred under the large cutting force in the cutting process, which made cemented carbide tool fracture along the direction of the edge. In this paper, based on the experimental phenomena, tool breakage degree is divided into slightly chipping, chipping, and breakage, and the flank breakage width is measured. For the first time to participate in milling, the sharp tool nose will break

when it contacts with the workpiece at the moment. So as to avoid causing the confusion for the different situation, in this paper, the tool breakage below 50μm is regarded as slightly chipping, which did not affect the milling process. The condition of tool breakage becomes increasingly serious with the milling progress. The tool breakage below 100μm is regarded as chipping, and the cutting state is close to the normal tool wear state. With the increase of tool breakage, the cutting force increase, the surface quality become worse, and the workpiece surface appear obvious cracks. When the tool breakage along the flank face reaches 200μm, the cutting condition is significantly serious, there is a large noise during the cutting process, and the burr phenomenon is obvious.At this time, the cutting temperature rises significantly, and the chip appears red around the cutting edge, resulting in workpiece surface quality is reduced, which is defined as tool breakage, as shown in Fig. 3.

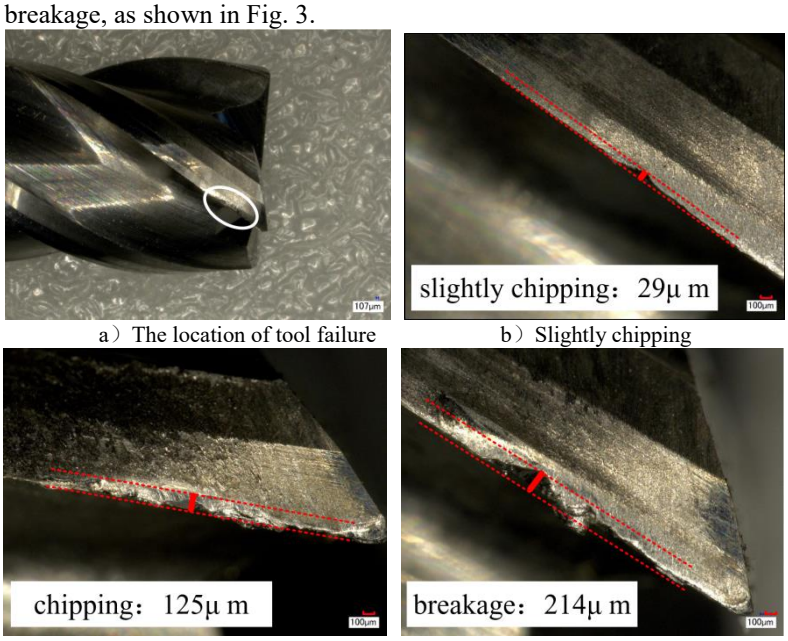

a）The location of tool failure　b）Slightly chipping

c）Chipping　d）Breakage

Fig. 3 Different degree of breakage

3.1 Tool material damage model

Before analyzing the damage mechanism of cemented carbide tool, the initial and critical damage values of tool material must be determined, which represents the damage state of the tool in the initial state and the limit state [30]. According to the existing researches, it can be known that the initial and the critical damage values are the inherent properties of tool material, in other words, these two values are independent of all external conditions. In order to determine the initial and critical damage values of tool material, a damage model is established for tool material. In the state of triaxial stress caused by external stress, the following assumptions are made: tool material damage is isotropic, there is initial cracks in tool material, and the crack propagation and joint eventually led to the tool damage failure.

Damage equivalent stress could be used to simplify the complex triaxial stress state into uniaxial stress state [31]. By equivalent transformation, the damage equivalent stress can produce the same elastic deformation energy density as the original triaxial stress state. It is assumed that the original triaxial stress state and the converted uniaxial stress state has the same effect on the damage evolution of tool material. Taking into account the quasi-unilateral condition of crack closure, the damage equivalent stress can be expressed as:

$$\sigma^{*}=\left\{\left(1+v\right)\left\langle\sigma\right\rangle^{+}:\left\langle\sigma\right\rangle^{+}-v\left\langle\mathrm{tr}\sigma\right\rangle^{2}+\frac{1-D}{1-h_{1}D}\left[\left(1+v\right)\left\langle\sigma\right\rangle^{-}:\left\langle\sigma\right\rangle^{-}-v\left\langle-\mathrm{tr}\sigma\right\rangle^{2}\right]\right\}^{1/2} \tag{17}$$

Where σ^{*} is the damage equivalent stress, σ is the triaxial stress, v is the Poisson's ratio of tool material, D is the damage value of tool material, the value of h_1 is 0.2.

Considering the computability of the model and the background of engineering application, the triaxial stress σ is related to the established cutting forces in this paper [31], where F_x, F_y, and F_z represented the average value of cutting forces in three directions X, Y and Z, the forces along X and Y direction contained impact force.

$$\sigma=\begin{bmatrix} \frac{F_x+F_{im,x}}{m^2} & 0 & 0 \\ 0 & \frac{F_y+F_{im,y}}{m^2} & 0 \\ 0 & 0 & \frac{F_z}{m^2} \end{bmatrix} \tag{18}$$

Further expression of the above formula, the external loading is expressed as damage equivalent stress σ^*, and the uniaxial compressional stress σ_c can be expressed as:

$$\sigma^*=\left(\frac{1-D}{1-h_1D}\right)^{1/2}|\sigma_c| \tag{19}$$

Substitute Equations (18) and (19) into Equation (20), and the forces act on tool material can be expressed as:

$$\sigma_c=\left\{(1+v)\langle\sigma\rangle^+:\langle\sigma\rangle^+-v\langle\mathrm{tr}\sigma\rangle^2+\frac{1-D}{1-h_1D}\left[(1+v)\langle\sigma\rangle^-:\langle\sigma\rangle^--v\langle-\mathrm{tr}\sigma\rangle^2\right]\right\}^{1/2}\left(\frac{1-D}{1-hD}\right)^{-1/2} \tag{20}$$

After the equivalent transformation of the stress state, the triaxial stress state could be transformed into the uniaxial compressive stress σ_c, and the stress state of the tool could be represented. The material element contains sliding microcracks originally. According to the simplified condition that the microcracks are uniformly distributed and interact each other, tool material damage could be solved in the next step.

In order to study the crack propagation of brittle material under compressive stress, many micro mechanical models have been established. The sliding crack model has been widely used by Horri and Nemat-Asser [32], and the sliding crack morphology is proposed to study the crack behavior under compressive stress. The open crack appears at the tip of the microcracks, and the curved microcrack is replaced by a straight line. The experimental results have shown that at the initial stage of crack propagation, the direction of crack propagation has a great angle with the axial compressive stress. After this initial stage, the crack propagates along the direction of axial compressive stress. Therefore, the sliding crack model is simplified and modified in Fig. 4. The crack expanded along the direction of the maximum axial compressive stress, and the initial microcrack length is $2c$, the crack length of each piece is l, the opening crack and the initial microcrack form an angle of θ, as shown in Fig. 4 [33].

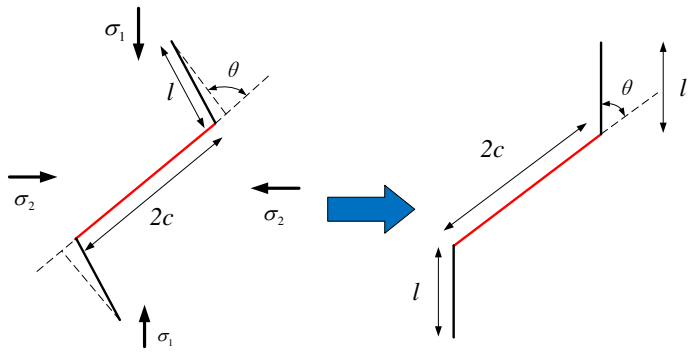

Fig. 4 Slip propagation model of single crack

According to existing researches [31], the interaction between cracks is taken into account, and a sliding crack model containing a sliding microcrack array under uniaxial compressive stress could be established. Strain ε_1 and ε_2 caused by the axial compressive stress σ_c.

$$\begin{pmatrix}\varepsilon_1\\ \varepsilon_2\end{pmatrix}=\begin{pmatrix}\varepsilon_1^{\,e}+\Delta\varepsilon_1\\ \varepsilon_2^{\,e}+\Delta\varepsilon_2\end{pmatrix} \tag{21}$$

Where $\varepsilon_1^e$and ε_2^e are the elastic strain of the non-damaged tool material, $\Delta\varepsilon_1$ and $\Delta\varepsilon_2$ are the total damage strain caused by the initial microcrack sliding and the sliding crack propagation.

The elastic strain of tool material without damage could be defined as:

$$\begin{pmatrix} \varepsilon_1^e \\ \varepsilon_2^e \end{pmatrix} = \frac{(k+1)(v+1)}{4E} \begin{bmatrix} 1 & \frac{k-3}{k+1} \\ \frac{k-3}{k+1} & 1 \end{bmatrix} \begin{pmatrix} \sigma_c \\ 0 \end{pmatrix} \tag{22}$$

Where E is the elastic modulus of tool material, K is the parameter determined by Poisson's ratio, K=5v for plane strain condition, and K=[(3-v)(1+v)] for plane stress condition.

According to Ravichandran and Chen [34], based on the consideration of the current linear problem, it is assumed that the damage strain is linearly related to the axial compressive stress applied externally σ_c, and there are N initial microcracks in tool material element, then the damage strain can be expressed as:

$$\begin{pmatrix} \Delta\varepsilon_1 \\ \Delta\varepsilon_2 \end{pmatrix} = N \begin{bmatrix} S_{11} & S_{12} \\ S_{21} & S_{22} \end{bmatrix} \begin{pmatrix} \sigma_1 \\ \sigma_2 \end{pmatrix} = N \begin{bmatrix} S_{11} & S_{12} \\ S_{21} & S_{22} \end{bmatrix} \begin{pmatrix} \sigma_c \\ 0 \end{pmatrix} \tag{23}$$

Where S_{11}, S_{12}, S_{21}, S_{22} are constants, and S_{12}=S_{21}, σ_1 and σ_2 are the normal stress in two directions in the plane.

If the interaction between microcracks is not taken into account, the above variables could be expressed by substituting them into the total damage strain. The total strain of the selected tool material element could be expressed as:

$$\begin{pmatrix} \varepsilon_1 \\ \varepsilon_2 \end{pmatrix} = \begin{pmatrix} \varepsilon_1^e + \Delta\varepsilon_1 \\ \varepsilon_2^e + \Delta\varepsilon_2 \end{pmatrix} = \frac{(k+1)(v+1)}{4E} \begin{bmatrix} 1 & \frac{k-3}{k+1} \\ \frac{k-3}{k+1} & 1 \end{bmatrix} \begin{pmatrix} \sigma_c \\ 0 \end{pmatrix} + N \begin{bmatrix} S_{11} & S_{12} \\ S_{21} & S_{22} \end{bmatrix} \begin{pmatrix} \sigma_c \\ \sigma_0 \end{pmatrix} \tag{24}$$

Let ε_1=ε, and the above equation can be simplified as follows:

$$\sigma_c = \frac{E}{1 + ENS_{11}} \varepsilon \tag{25}$$

Under the condition of external loading, the strain of the damaged material is controlled by the elastic modulus E. The elastic modulus is the inherent parameter of tool material. With the milling process, the damage of tool material is continuously to accumulated, and the elastic modulus is also reduced. Therefore, the elastic modulus of tool material degradation is used to define the damage of the material element [31]:

$$\sigma_c = E_D \varepsilon = E(1-D)\varepsilon \tag{26}$$

$$D = 1 - \frac{E}{1 + ENS_{11}} \tag{27}$$

The damage value of tool material and elasticity modulus with degradation could be respectively solved to get elastic strain energy W_e caused by the open crack propagation, the frictional energy W_f caused by the initial microcracks and the work done W_1 caused by the uniaxial compressive stress [31].

The work done W_1 can be expressed as:

$$W_1 = 4ab(\sigma_1\varepsilon_1 + \sigma_2\varepsilon_2) = 4abS_{11}\sigma_c^{\,2} \tag{28}$$

Where 2a and 2b are the lengths of the selected unit, which is the same order of magnitude as the crack length.

Furthermore, the stress intensity factor of the crack array could be calculated according to the existing studies:

$$\begin{cases} K = F_1 \sin\theta [w \sin \dfrac{\pi(l_n + l_1)}{w}]^{-1/2} \\ F_1 = 2c * \tau_m \\ \tau_m = \dfrac{1}{2}\sigma_c \sin 2\theta - \dfrac{1}{2}\mu[\sigma_c - \sigma_c \cos 2\theta] \end{cases} \tag{29}$$

Where τ_m is the shear stress leading to the initial crack slip, μ is the friction coefficient, F_1 is the shear force caused the initial crack to slip.

$$l_n = l_{n-1} + \dot{l}_n \Delta t \tag{30}$$

Where $l_1 = 0.27c_1$, l_1 is used to correct the small crack length, l_n is the length of the nth impact cracks, and $2w$ is the spacing between microcracks. Even in the early stage of crack propagation, the calculation results of the stress intensity factor could be kept accurate [35].

Paris fatigue crack propagation formula can be used to describe the relationship between the stress intensity factor from the crack tip and the crack propagation rate:

$$\dot{l}_n = \frac{dl}{dn} = C_1(\Delta K)^{m_1} \tag{31}$$

Where n is the number of stress cycles and also is the number of cutting of each tooth, both C_1 and m_1 are material constants, which can be obtained by fitting according to experimental data.

The tool fatigue damage is divided into the process of crack initiation and crack propagation, as shown in Fig. 5. The crack propagation rate is denoted by dl/dn, and the control parameter of crack propagation rate is denoted by the crack tip stress intensity factor amplitude ΔK. In region I, the value of ΔK is far less than the fatigue crack threshold value ΔK_{th}, so tool material have no crack propagation, but with the continuous damage of tool material, crack propagation strength will also continue to increase, when it more than the critical value, the crack will enter into the propagation stage. At this stage, dl/dn is approximately proportional to ΔK. In region II, since dl/dn -ΔK increases with an approximately constant change rate, the cracks within this region are in a state of stable propagation. When ΔK continues to increase and the maximum stress at the crack tip exceeds the critical propagation stress, the crack propagation rate increases sharply and the crack propagation becomes unstable. The macroscopic manifestation is that the material can no longer maintain its own physical properties at this time and the material will fracture rapidly [36].

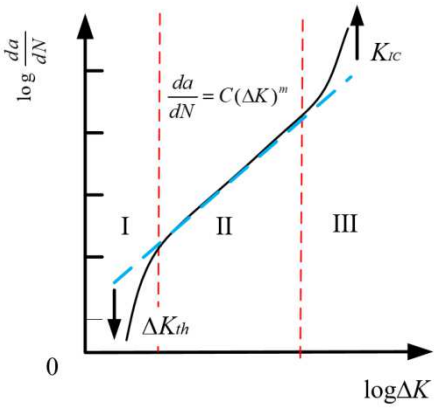

Fig. 5 The relationship of dl/dn-ΔK

According to the above, it could be known that the variation trend of crack length with the number of cyclic loading, as shown in Fig. 5. The relationship between crack propagation rate dl/dn and stress intensity factor ΔK is described by Paris formula [36]:

$$\frac{dl_n}{dn} = 8.3112 \times 10^{-16} (\Delta K)^{10.71} \tag{32}$$

Where dl_n/dn is the crack propagation rate of tool material under the nth impact.

$$W_e = 2\int_0^{l_n} \frac{(k+1)(v+1)}{4E} K^2 dl \tag{33}$$

$$W_f = 2c\tau_f \chi \tag{34}$$

Where τ_f is the shear traction on the crack surface caused by uniaxial compressive stress, χ is the sliding distance of the initial microcrack faces [30].

$$\chi = \frac{(k+1)(v+1)}{4E} c\tau_f [w \sin \frac{\pi(l_n + l_1)}{w}]^{-1/2} [2\pi(l_n + l_1)] \tag{35}$$

$$\tau_f = \frac{1}{2}\mu[\sigma_c - \sigma_c \cos 2\theta] \tag{36}$$

$\dot{l}_0$ and l_0 are respectively the initial damage value of tool material and the initial crack propagation rate. After tool material bears nth impacts, the damage value of tool material is D_n and the crack propagation length is l_n. Determine the damage value D_n and crack opening propagation length l_n is the initial condition when tool material is subjected to (n+1) impacts.

$$2W_e + W_f = W_1 \tag{37}$$

Substitute Equations (28) and (33) into Equation (37) to get S_{11} and the damage value and the expression after the damage are obtained.

3.2 The initial and critical damage value of tool material with interval method

Since the crack related parameters in the initial damage state cannot be accurately determined, the interval method is adopted in this paper to cover the length value of the crack length in the initial damage state as much as possible, and the interval method is used to solve the damage value and the degenerated elastic modulus obtained above.

Cemented carbide is made of cobalt (Co), nickel (Ni), molybdenum (Mo), and other elements bonded to micron powder of high hardness metal and processed at high temperature. According to existing studies, it can be assumed that $2c=d$, where d is the particle size of tool material. Sandvik classified the particle size of hard alloy crystal as shown in Table 1. The particle size of the cemented carbide used in the experiment is medium to fine, about 1μm to 2μm. For the angle θ of the propagation direction of all microcracks is taken as $\pi/4$, the interval method is used to calculate the initial crack spacing of $2w$, which is 4 times as many as the crack length [37].

Table 1 Grain size grading standards of cemented carbide of Sandvik

Grain grade	Grain size of the WC (μm)	Grain grade	Grain size of the WC (μm)
ultrafine	0.3 ~ 0.5	very fine	0.5 ~ 0.9
fine	1.0 ~ 1.3	medium	1.4 ~ 2.0
medium coarse	2.1 ~ 2.4	coarse	3.5 ~ 4.9

The interval number represents a number set, and the maximum and minimum values of the number set are used as endpoints to describe the interval number. The maximum and minimum values of the real number set are expressed by $\overline{X}$ and $\underline{X}$ in the number set, where $\overline{X} < \underline{X}$, then the bounded real number set can be expressed as [38]:

$$X^1 = [\underline{X}, \overline{X}] = \left\{ X \mid X \in R, \underline{X} \le X \le \overline{X} \right\} \tag{38}$$

The calculation of interval number is based on the algorithm of the set. The addition and subtraction of two interval numbers are added and subtracted between all elements in the two interval numbers. The upper and lower bounds of the interval number obtained by multiplying the interval numbers are respectively the maximum and minimum values of the two interval numbers' endpoints.

$$X^1 + Y^1 = \left[\underline{x}, \overline{x}\right] + \left[\underline{y}, \overline{y}\right] = \left[\underline{x} + \underline{y}, \overline{x} + \overline{y}\right] \tag{39}$$

$$X^1 - Y^1 = \left[\underline{x}, \overline{x}\right] - \left[\underline{y}, \overline{y}\right] = \left[\underline{x} - \underline{y}, \overline{x} - \overline{y}\right] \tag{40}$$

$$X^1 \times Y^1 = \left[\underline{x}, \overline{x}\right] \times \left[\underline{y}, \overline{y}\right] = (\left[\min(M), \max(M)\right], M = \underline{x}\underline{y}, \underline{x}\overline{y}, \overline{x}\underline{y}, \overline{x}\overline{y}) \tag{41}$$

$$X^1 / Y^1 = \left[\underline{x}, \overline{x}\right] / \left[\underline{y}, \overline{y}\right] = \left[\underline{x}, \overline{x}\right] \times \left[\frac{1}{=}, \frac{1}{\underline{y}}\right] (0 \notin \left[\underline{y}, \overline{y}\right]) \tag{42}$$

In the process of crack propagation, the density of initial crack and the number of initial crack have important effects on the tool damage. The initial crack density is defined as follows:

$$f_0 = N_0 c^2 \tag{43}$$

$$N_0 = \frac{4abP}{c^2} \tag{44}$$

Where f_0 is the density of the initial crack, N_0 is the number of initial microcracks in the unit area, and P is the porosity of cemented carbide.

Cemented carbide belongs to powder metallurgy material, and there is an adhesive is inevitably the existence of micro-pores and other microscopic defects, so that the tool in the original state has a certain damage, cemented carbide material porosity calculation formula [36]:

$$P = \left(1 - \frac{\rho}{\rho_0}\right) \times 100\% \tag{45}$$

Where ρ is the actual density of cemented carbide, and ρ_0 is the nominal density of cemented carbide.

It can be seen from the above formula that the damage value of tool material D decreases with the increase of crack length. For fixed tool material, although the initial and critical damage of tool material is an inherent property of tool material, but also influenced by the crack propagation in the tool initial state. The crack propagation speed is determined by the frequency and strength of the external cyclic loading. Because the initial propagation rate is low, the influence of crack propagation speed on the initial damage value and critical damage value of tool material is ignored in this paper.

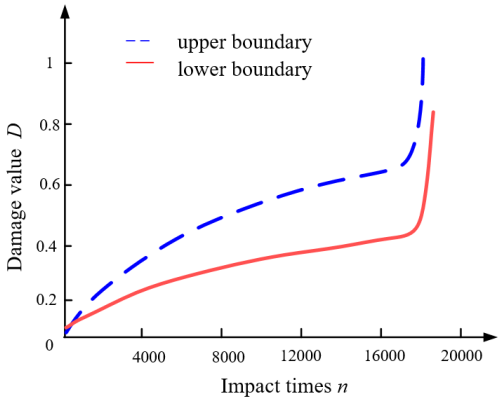

Fig. 6 The damage value of tool varies with impact times

As shown in Fig. 6, damage value of tool material at the starting point is 0.0175, and the damage value at this point is considered to be tool material initial damage value D_0, which is determined by the properties of tool material. The tool have small defects in the casting process, which leads to a certain amount of damage to the tool in not cutting stage. The damage value is measured by [0.0175, 0.0314], and the initial damage value is extremely small. According to the existing parameters, it can be seen that when the number of impacts on the tool reaches about 20,000 times, damage value of tool material has an obvious rising stage, which proves that tool material reaches a critical value this is between [0.41, 0.58] at this time. There is obvious damage inside tool material, the length of the crack reaches the critical value, and the tool life reaches the limit, the tool damage value is between [0.41, 0.58], and there is a very high possibility of cutting edge fracture at any moment.

3.3 Degradation of elastic modulus

The elastic modulus is a physical quantity that describes the material resistance to elastic deformation. The elastic modulus of tool material will vary with the type of material such as hot working technology, cold plasticity, and other factors [31]. When the tool is milling, under the impact of continuous cyclic loading, the crack in tool material expands, which increases the damage degree of tool material and changes the elastic modulus. The degenerated elastic modulus can be expressed by the damage value of tool material:

$$\sigma_c = E_D \varepsilon = E(1 - D)\varepsilon \tag{46}$$

Milling belongs to intermittent cutting, so the cutting time of each tooth starts from the tool cutting into workpiece to the end of the tool cutting out workpiece. Therefore, the cutting time is determined by the cutting speed and immerse angles. The effective cutting time of each tool tooth can be expressed as:

$$\Delta t = \frac{\theta_{ex} - \theta_{en}}{2\pi} t \tag{47}$$

Where θ_{en} is the cutting entry angles, θ_{ex} is the cutting exit angles, Δt is effective cutting time.

By substituting the above formula, the changing trend of the tool elastic modulus with time in the

milling process can be obtained:

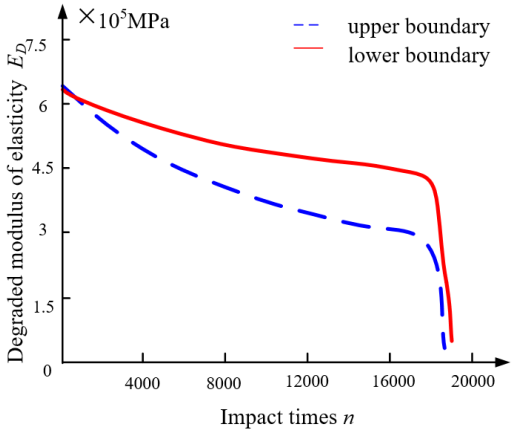

Fig. 7 The elastic modulus of tool varies with impact times

As shown in Fig. 7, the elastic modulus presents a downward trend with the number of impacts. Under the existing cutting conditions, when the number of impacts that the tool bears under the cyclic loading approaches 20,000 times, the elastic modulus shows a sharp decline, which proves that the tool is in a severe damage state at this time.

3.4 The limit fracture conditions with tool cutting impact

The milling process of cemented carbide tool is the intermittent cutting state. In the air stroke into the cutting workpiece state, the tool will be subjected to greater impact, at this time the cemented carbide tool is limited to low impact resistance and toughness ability, so that its usable life is significantly reduced. The tool will go through the process of cutting into and cutting out workpiece. In down-milling, workpiece and tool teeth collide at a certain angle at the beginning of tooth contact workpiece, This process is depicted by a tool-workpiece contact model with a single degree of freedom in italic collision [28]. On the basis of considering the cutting impact force and combining with the milling force model of workpiece material hardness, the cyclic loading that the cemented carbide tool must bear in milling titanium alloy can be obtained.

The magnitude of the tool cutting-in impact force is mainly determined by the relative contact velocity when the tool collides with the workpiece and the depth of the tool cuts into workpiece. Therefore, it is assumed that there is no energy loss during the impact process, that is, the kinetic energy during the impact process is all converted into the energy used for the fracture of the tool tooth, resulting in tool damage. Then, on the basis of considering the tool impact fracture, the critical condition of the impact fracture of the cemented carbide tool is [39]:

$$F_{zong} \geq \tau A = G\gamma A \tag{48}$$

Where F_{zong} is the overall impact force obtained on the basis of considering the tool cut-in impact, G is the shear modulus of cemented carbide tools, γ is the shear strain of cemented carbide in the process of impact fracture, A is the cross-sectional area of the fracture.

Due to the randomness of the location and size of the tool breakage in the cutting process, an irregular fracture area graph is generated at this time. The height of the cross-sectional area can be approximated as the cutting depth, and the width of the tool breakage is a wide parallelogram. The area can be expressed as:

$$A = m \cdot VB_{po} \cdot a_p \tag{49}$$

Where VB_{po} is the width of tool flank breakage, a_p is the cutting depth, m is the fracture area parameter obtained by experiment.

According to the shear Hook's law, the shear modulus of cemented carbide tools can be expressed by elastic modulus E and Poisson's ratio v:

$$G = \frac{E}{2(1+v)} \tag{50}$$

In considering the cut-in impact state, with the continuous cutting, tool material is continuously damaged, and the tool impact fracture conditions can be obtained:

$$F_{zong} \geq \frac{\gamma m E_D V B_{po} a_p}{2(1+v)} \tag{51}$$

$$\xi \geq [\tau] = \frac{E_D \gamma}{2(1+v)} \tag{52}$$

Where ξ is impact stress, γ is shear strain of cemented carbide, $[\tau]$ is allowable stress in the process of tool impact, E_D is elastic modulus after tool damage.

The impact fracture boundary of tool breakage failure is simulated by selecting 0.2mm tool breakage along the flank face as the criteria of tool breakage failure. The specific simulation results are shown in Fig. 8.

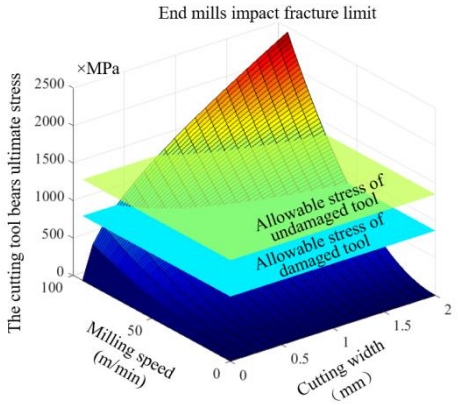

a)The relation between cutting speed, cutting width and the loading of the tool

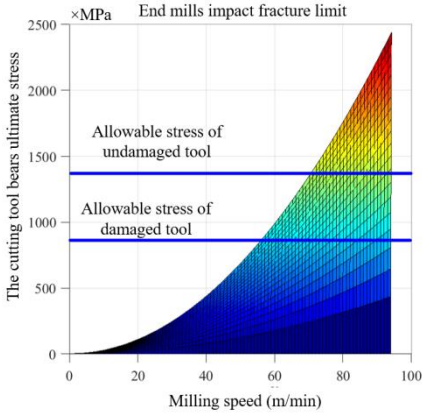

b)The relation between cutting speed and the loading of the tool under different cutting widths

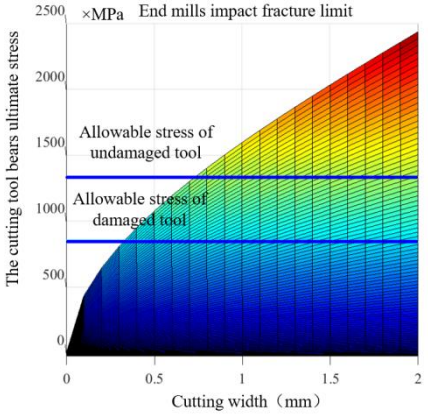

c)The relation between feed and tool loading under different cutting speeds

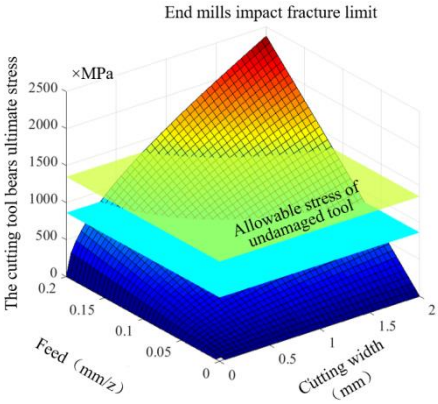

d)The relation between feed and cutting width and the loading of the tool

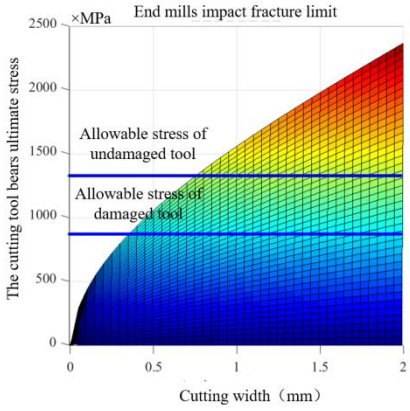

e)The relationship between cutting width and loading of the tool under different feed

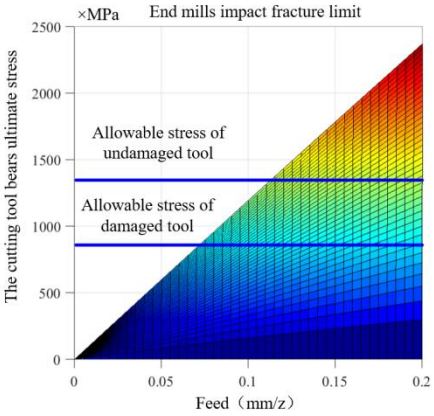

f)Relation between feed and tool loading at different cutting widths

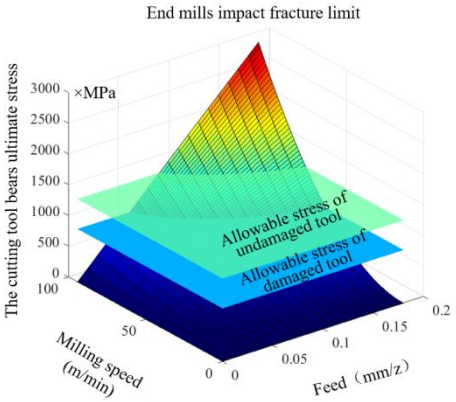

g)The relationship between cutting speed, feed and the loading of the tool

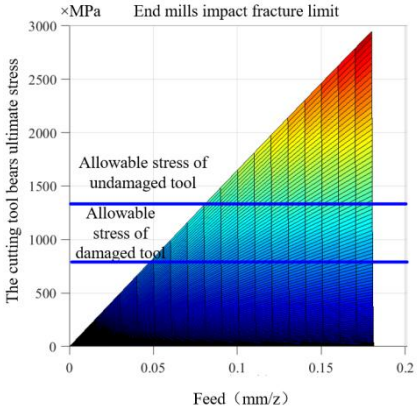

h)The relation between feed and tool loading at different cutting speeds

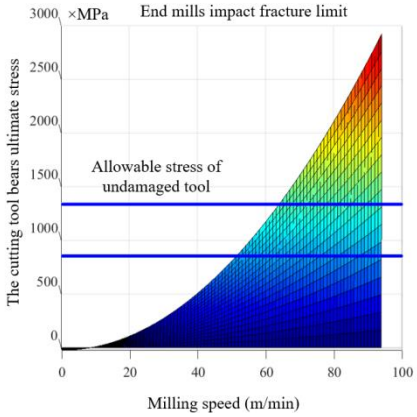

i)The relationship between cutting speed and tool loading under different feed

Fig. 8 Diagram of feed, cutting speed, cutting depth and tool impacting on fracture loading

As shown in Fig. 8, the impact fracture loading of the tool shows an upward trend with the increase of the feed per tooth, the cutting speed and the cutting width in the cutting process. Through c) and e) in Fig. 8, considering the vertices of the upper limit of the curve affected by the three factors, the relationship between the tool impact fracture loading and the cutting width can be expressed by the quadratic function with lower slope *k*, which will increase with the decrease of the cutting width, and become larger when the cutting width is below 0.2mm. When the cutting width is large and the slope is small, the cutting speed shows a sharp rise in the approximate quadratic power relationship for the loading borne by the tool, indicating that the loading borne by the tool is more obvious in the cutting process. It can be seen from b) and i) in Fig. 8 that the loading on the tool and the cutting speed are expressed by an approximate quadratic function. And in Fig 8 f) and h), the relationship between the loading and the tool feed can be seen as approximately linear, and the curve of the tool impact fracture loading and the feed also changes at different cutting speeds. With 50 m/min as the boundary, when the cutting speed does not reach this boundary, the curve can be regarded as linear curve, and the curve has a slight change. When the cutting speed exceeds this boundary, the curve can be regarded as a quadratic function curve. When the cutting depth is 0.08 mm, there is a rapid rise stage.

There are two planes in Fig. 8 a)-i). The upper plane is the ultimate allowable stress when the tool is not damaged, and the lower plane is the ultimate allowable stress that the tool can withstand when reaching the critical state after a period of cutting. As shown in Fig. 8, the ultimate allowable stress that the tool can withstand after damage is significantly reduced, indicating that the crack length inside the tool has extended to the critical state.

According to the impact fracture critical model and the force and damage value of cemented carbide tool in high speed milling of titanium alloy, the critical value of impact fracture can be determined. Therefore, the impact fracture damage of cemented carbide tool has time-varying characteristics. As shown in Fig. 9, after the predicted cutting time, the tool damage is solved firstly. The ultimate stress loading that the tool can withstand before and after the damage is compared. The loading that the tool can withstand during the impact fracture of cemented carbide tool and the loading that the tool needs to withstand under different damage states are extracted. According to the graphical curve, the cutting parameters in the safety range can be given. The part below the curve in Fig. 9 is the safety area, in which

the tool can be ensured not to break in the predicted tool life time.

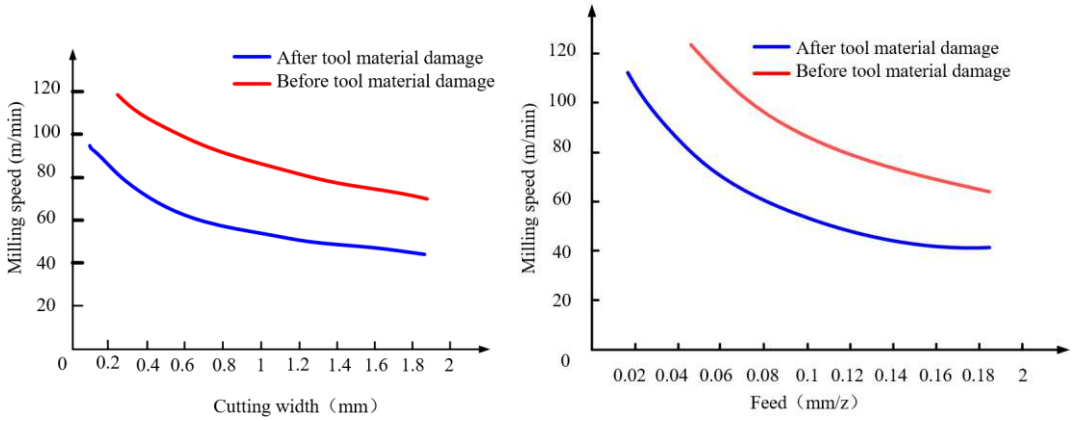

(a) Relationship between cutting width and cutting speed (b) The relationship between feed and cutting speed

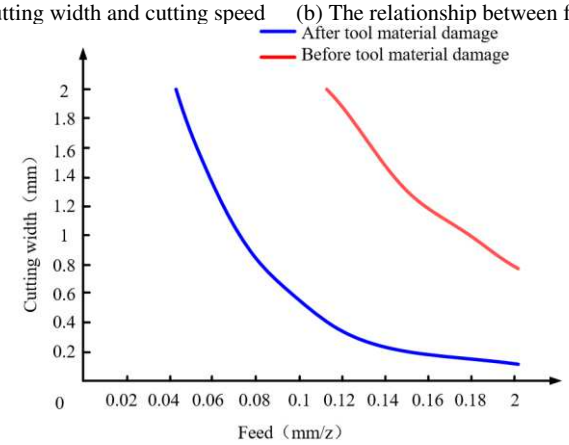

(c) relationship between cutting width and feed

Fig. 9 Safety range of milling parameters

As shown in Fig. 10, the three axes of the spatial coordinate system are cutting depth, cutting speed and feed rate. The three axis coordinate system is selected to verify the safety curve of the cutting process of tool material [40], which can effectively avoid the occurrence of impact fracture in the specified time.

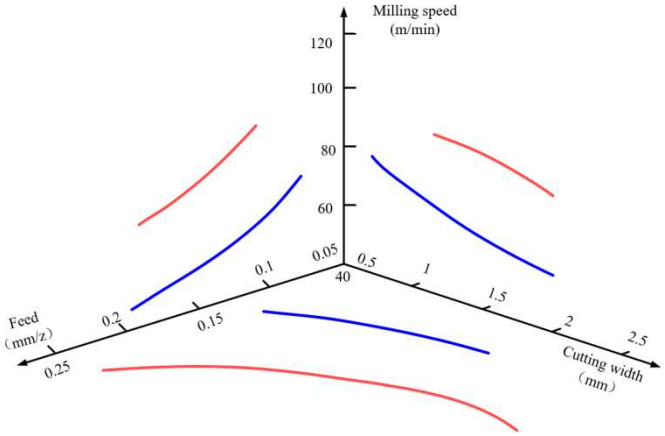

Fig. 10 Safety range of milling parameters based on avoiding breakage

3.5 Experimental verification of tool breakage analytical model

The three-axis CNC machine tool VDL-1000E produced by Dalian Machine Tool Group is used in the experiment, and the dry milling method is used. The experimental tool is flat bottom uncoated end mill, which material is YG6 cemented carbide; The force is measured by Kistler 5236B rotary dynamometer; Using milling tool tooth number N is 4, diameter D is 10mm, spiral angle λ_s is 35° ; The experimental workpiece material is titanium alloy Ti6Al4V for aviation, and the size is 100×100×100mm; The side milling parameters are shown in Table 2.

Table 2 The experimental cutting parameters

Experimental cutting parameters						
Experimental Samples	v (m /min)	a_e (mm)	a_p (mm)	f_z (mm/z)	Failure time	Damage length
1	130	1	3	0.15	94.2	201
2	100	1	3	0.15	117	214
3	80	1	3	0.15	321	241
4	80	1	3	0.08	313	200
5	80	1.5	3	0.08	207	213
6	47.12	1	3	0.08	--	--

The test site diagram of milling titanium alloy with cemented carbide end milling tool is shown as follows:

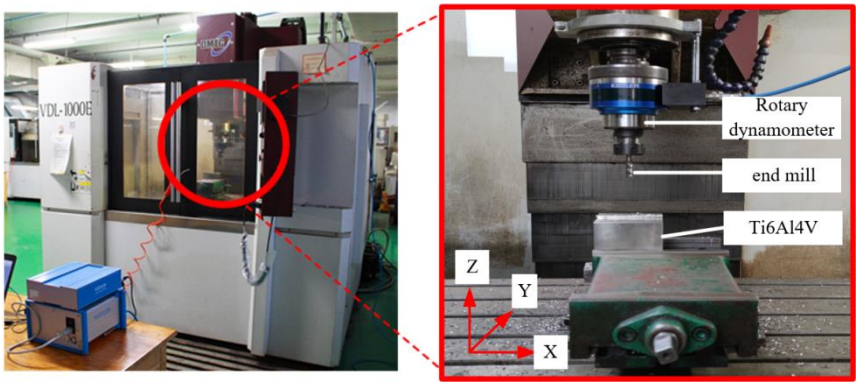

Fig. 11 The test site diagram

The cutting parameters can be selected from the text to ensure the reliability of the tool under large cutting parameters. In order to realize the effective value of the critical cutting parameters of impact fracture more effectively, and make the range of the shadow part within the range specified by the three curves. The tangent of the curve is drawn, and the safety area is verified by different parameter points in Table 2, as shown in Fig. 12.

As shown in Fig 12, the safety curve of tool material after damage is further divided. When the cutting speed is determined to be 83 m/min, according to the corresponding safety area, the maximum cutting width can be obtained about 2 mm. When the cutting speed is determined to be 83 m/min, the maximum value that can be achieved according to b) in Fig. 9 is about 0.13mm/z. At this time, the cutting parameters are selected: cutting speed 70m/min, feed 0.1mm/z. In order to verify the rationality of the cutting parameters, the corresponding experimental cutting parameters are substituted into Fig. 12, and the landing point is in the safety area. It shows that the selected cutting parameters are safe and can effectively avoid the occurrence of impact fracture in the specified time.

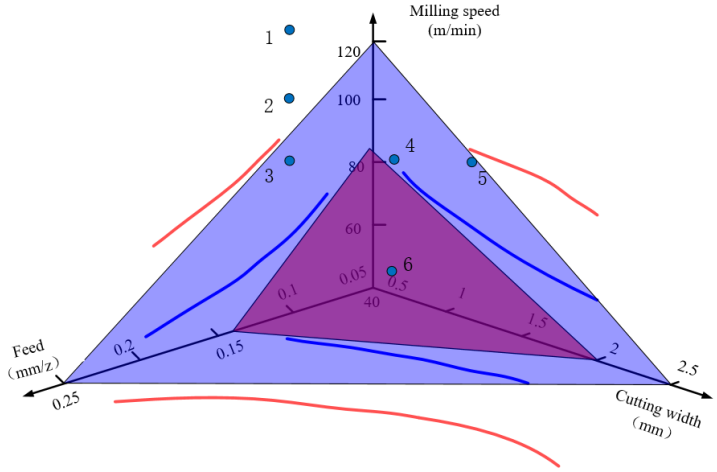

Fig. 12 The optimized safety range of milling parameters based on avoiding breakage

The parameters in the shadow can ensure that the cemented carbide tool does not break 200μm in the predicted tool life achieved 300s in Fig. 12. As shown in Fig. 12, with the cutting process, the tool continues to be damaged, and safety range of tool cutting parameters will be reduced. According to the cutting parameters, the prediction safety area of tool breakage is verified. The selected tool breakage

measurement position is 0.5 times the depth along the end mill to participate, and the measurement is carried out along the flank breakage direction. As shown in Fig 13, No.1, 2, 5 experimental parameters are located outside the safety range. Severe damage has occurred in less than 300s, and the breakage length along the flank reaches 200μm. No.3, 4 experimental parameters are located in the upper and lower boundaries of the safety experimental parameters, and the breakage length along the flank reaches 200μm in the continuous cutting of about 300s. No.6 experimental parameter is located in the range of safety parameters, and there is no broken. The tool damage evolution is characterized in the form of tool flank breakage.

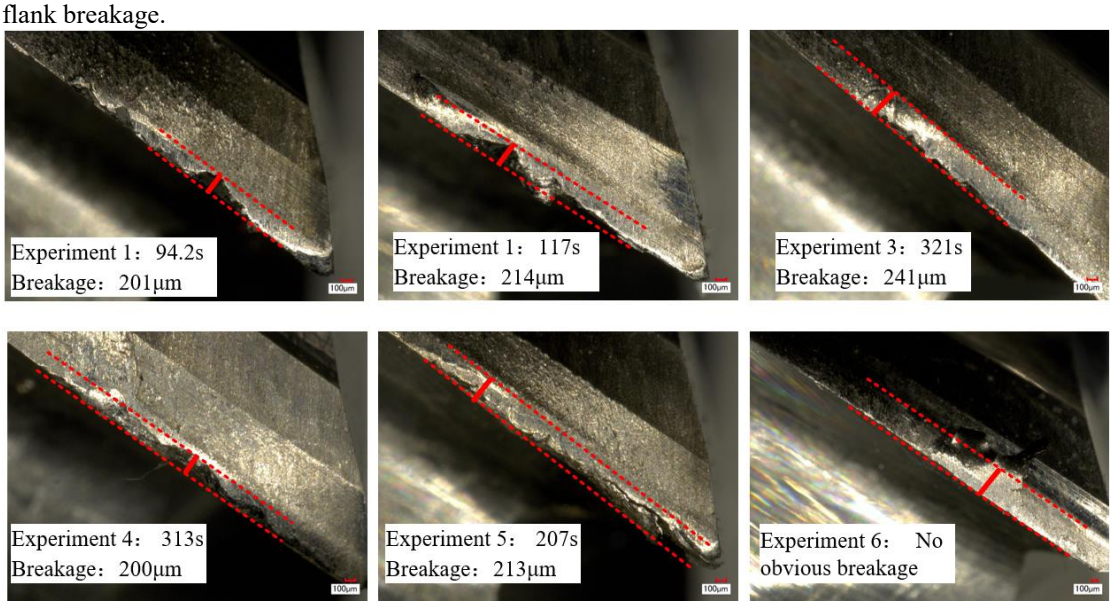

Fig. 13 The result of the experiment

Due to the matrix of cemented carbide tool is powder metallurgy, cracks and defects are randomly distributed. Because the intermittent cutting is a complex process in the cutting process, the mechanical shock and thermal shock on the tool randomly occur, which causes the fatigue propagation of the crack core inside the tool and finally leads to the tool breakage. There is a certain contingency in the occurrence of tool breakage. In addition, the interval coverage of the initial value will have a certain impact on the final prediction results.

4 Conclusion

The large thermal-mechanical loading lead to serious cemented carbide tool breakage in the milling of titanium alloy, which also caused the low machining efficiency. This paper studied the material damage model of cemented carbide tools with high speed milling of titanium alloy, and studies the influence of tool damage of tool breakage from the perspectives of theory, experiment and simulation. It is found that the tool exhibits the characteristics of damage accumulation and sudden fracture. The critical condition of tool impact fracture is established, and the conclusions are as follows:

1. According to the research results of the tool damage mechanism, the tool damage accumulation will also occur when the tool cuts into the workpiece, and tool material fracture is more likely to occur. The tool-workpiece contact model is introduced as the single-degree of freedom italic collision model to describe the cutting impact in the milling process.
2. The occurrence of damage accumulation can be attributed to the propagation of the microcracks between the cutting tool material grains. Based on the continuum damage mechanics, the interval method is adopted to cover the uncertain parameters in the model of the initial crack length, which eventually get the tool damage evolution and crack length and curves of relationship between carbide materials. The initial and critical damage values of cemented carbide material are [0.0175, 0.0314] and [0.41, 0.58] respectively. It is also found that when the crack length reaches a threshold value, the damage values of tool material rise rapidly, and the elastic modulus decreases sharply.
3. According to the cutting tool under cyclic loading characteristics and damage mechanics, the impact fracture limit condition is established including cutting parameters and material hardness of the end mill, the degree of the end mill breakage is defined, and the safety area of the tool breakage is divided, which provide support for optimizing cutting parameters of high efficiency milling of

titanium alloy.

Acknowledgements

This project is supported by Projects of International Cooperation and Exchanges NSFC (Grant Number 51720105009), National Key Research and Development Project (Grant Number 2018YFB2002201), and Outstanding Youth Fund of Heilongjiang Province (Grant Number YQ2019E029)

References

1. Chen L, Zhang XM, Ouyang P (2015) A life prediction model for low cycle fatigue based on continuum damage mechanics. China Mechanical Engineering 26(18): 2506-2517
2. Zhang CY, Lu JP, Zhang FP, Butt SI (2017) Identification of a new friction model at tool-chip interface in dry orthogonal cutting. The International Journal of Advanced Manufacturing Technology 89(1-4): 921-932
3. Girolamo GD, Pilloni L, Pulci G, et al (2009) Tribological characterization of WC-Co plasma sprayed coatings. Journal of the American Ceramic Society 92(5): 1118-1124
4. Huang DY, Yi DQ, Liu HQ, Cai ZG, Liu R, Li J (2007) Effect of temperature on bending strength and failure mechanism of cemented carbide. Transactions of material and Heat Treatment 8(5): 105-108
5. Chandrasekaran H, Venkatesh VC (1985) Thermal fatigue studies on tool carbides and its relevance of milling tools. Elsevier 34(1): 125-128
6. Gee M, Mingard K, Roebuck B (2008) Application of EBSD to the evaluation of plastic deformation in the mechanical testing of WC/Co hardmetal. International Journal of Refractory Metals and Hard material 27(2): 300-312
7. Llanes L, Torres Y Anglada M (2002) On the fatigue crack growth behavior of WC-Co cemented carbides: kinetics description, microstructural effects and fatigue sensitivity. Acta Materialia 50(9): 2381-2393
8. Chivavibul P, Watanabe M, Kuroda S et al (2007) Effects of carbide size and Co content on the microstructure and mechanical properties of HVOF-sprayed WC-Co coatings. Surface&Coatings Technology 202(3): 509-521
9. Uhlmann E, Sammler F, Meixner M, et al (2015) Analysis of residual stresses andwear mechanism of HF-CVD diamond coated cemented carbide tools. Production Engineering 9(1): 99-107
10. Torres Y, Anglada M, Llanes L (2001) Fatigue mechanics of WC-Co cemented carbides. International Journal of Refractory Metals and Hard material 19(4-6): 341-348
11. Chivavibul SM, Pandey PC (1978) Thermal cracking of carbide tools during intermittent cutting. Wear 51(2): 201-211
12. Jiang Y, Li ZQ, Zhong YP, Chen ZH (2012) On the fatigue and fracture features of WC-Co cemented carbides. Powder Metallurgy Technology 30(5): 341-347
13. Pekelharing A J (1979) Cutting tool damage in interrupted cutting. Wear 62(1): 37-48
14. Feng M, Chen YJ, Ni L (2007) Research status and development tendency of the mechanism of tool fracture. Cemented Carbide 24(01): 39-41
15. Gong F, Zhao J, Jiang YW, et al (2017) Fatigue failure of coated carbide tool and its influence on cutting performance in face milling SKD11 hardened steel. International Journal of Refractory Metals and Hard material 64: 27-34
16. Li ZJ, Li ZR, Yi B, et al (1993) Study on cause of milling tool destruction. Journal of Mechanical Engineering 29(4): 93-96
17. Ni XY, Zhao J, Gong F, Li G (2020) Fatigue failure analysis of ceramic tools in intermittent cutting harden steel based on experiments and finite element method. Proceedings of the Institution of Mechanical Engineers, Part B: Journal of Engineering Manufacture 234(4): 692-700
18. Liu B, Zhu ZX, Zhang J, Lei WN, Wu BC (2018) Fatigue failure analysis of drilling tools for ultra-deep wells in shunbei Block. IOP Conference Series: material Science and Engineering 423(1): 012190
19. Ding CG, Liu XQ, Li Y, et al (2013) Study on fracture of the fibrous monolith cemented carbide. Advanced material Research 815: 43-47
20. Doi S, Yasuoka M (2009) Fracture toughness KIC of cemented carbide WC-Co. WIT Trans Eng Sci 64: 217-226
21. Yan L, Wang XB, Zhang LS, Liu XL, Ding MH (2019) Simulation analysis of micro milling tool

breakage failure factors. Small & Special Electrical Machines 47(09): 69-72
22. Gong F, Zhao J, Ni XY, Liu CX, Sun JL, Zhang QZ (2019) Wear and breakage of coated carbide tool in milling of H13 steel and SKD11 hardened steel. SN Applied Sciences 1(9): 1-12
23. Yuan Q, Cheng Y, Wang ZH, Hu X (2019) Study on tool failure of carbide tools in turning γ-TiAl alloy. Tool Engineering 53(02): 12-16
24. He GH (2013) Research on both the high-efficiency cutting of large shell and the tool technology. Dissertation, Harbin University of Science and Technology
25. Wang XG, Lu CM, Wang BY, Yan MM (2015) Research on dynamic reliability and failure rate of cemented carbide cutting tool. Journal of Northeastern University(Natural Science) 36(6): 843-847
26. Wang XQ, Ai X, Zhao J, et al (2008) Experimental investigation on cutting force and tool wear of carbide tools in Ti6A14V turning. Key Engineering material 375: 231-235
27. Sun YJ (2014) Parametric modeling of milling titanium alloy and prediction of tool wear state. Dissertation, Shandong University
28. Gao HN (2019) Research on milling process and cutting parameters inversion of splicing die with different hardness. Dissertation, Harbin University of Science and Technology
29. Altan E, Uysal A, Anal SH, et al (2017) Effect of work hardening of cobalt in sintered carbide cutting tool on tool failure during interrupted cutting. The International Journal of Advanced Manufacturing Technology 88(1-4): 359-367
30. Cui XB, Zhao J, Pei ZQ (2012) Analysis of transient average tool temperatures in face milling. International Communications in Heat and Mass Transfer 39(6): 786-791
31. Cui XB (2013) Tool failure mechanisms in high-speed intermittent cutting of hardened steel. Dissertation, Shandong University
32. Horii H, Nemat-Nasser S (1986) Brittle failure in compression: splitting, faulting and brittle-ductile transition. Philosophical Transactions of the Royal Society of London. Series A, Mathematical and Physical Sciences 319(1549): 337-374
33. Wang C (2018) Study on fatigue damage characteristics of heavy milling cemented carbide tools. Dissertation, Harbin University of Science and Technology
34. Ravichandran G, Chen W (1991) Dynamic failure of brittle material under uniaxial compression. Experiments in Micromechanics of Fracture Resistant material 131:85-90.
35. Ashby MF, Hallam SD (1986) The failure of brittle solids containing small cracks under compressive stress states. Acta Metallurgica 34(3): 497-510
36. Liu L (2018) Damage evolution process and failure mechanism of carbide insert during milling water chamber head. Dissertation, Harbin University of Science and Technology.
37. Bai X, Tu BY, Wang K, Zhao CY (2020) Interval non-probabilistic reliability analysis of fatigue crack growth in titanium alloys. Journal of Ship Mechanics 24(08): 1055-1061
38. Kemeny JM (1991) A model for non-linear rock deformation under compression due to sub-critical crack growth. International Journal of Rock Mechanics and Mining Sciences & Geomechanics Abstracts 28(6): 459-467
39. He GH (2013) Research on both the high-efficiency cutting of large shell and the tool technology. Dissertation, Harbin University of Science and Technology.
40. Guan R (2017) Research on damage characteristics of cemented carbide tools for milling high strength steel. Dissertation, Harbin University of Science and Technology

Figures

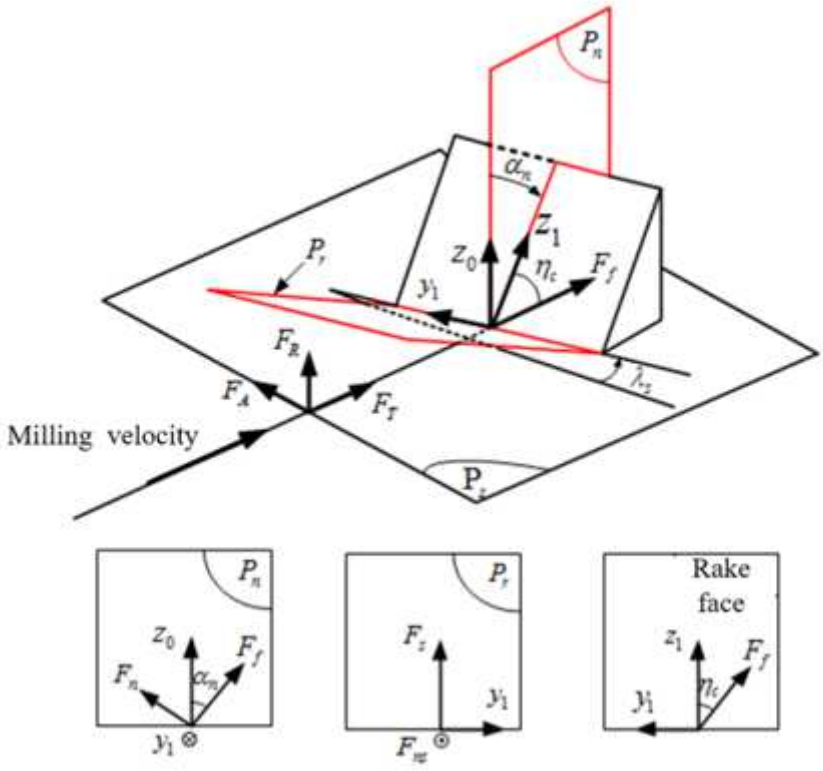

Figure 1

The forces in the oblique cutting area

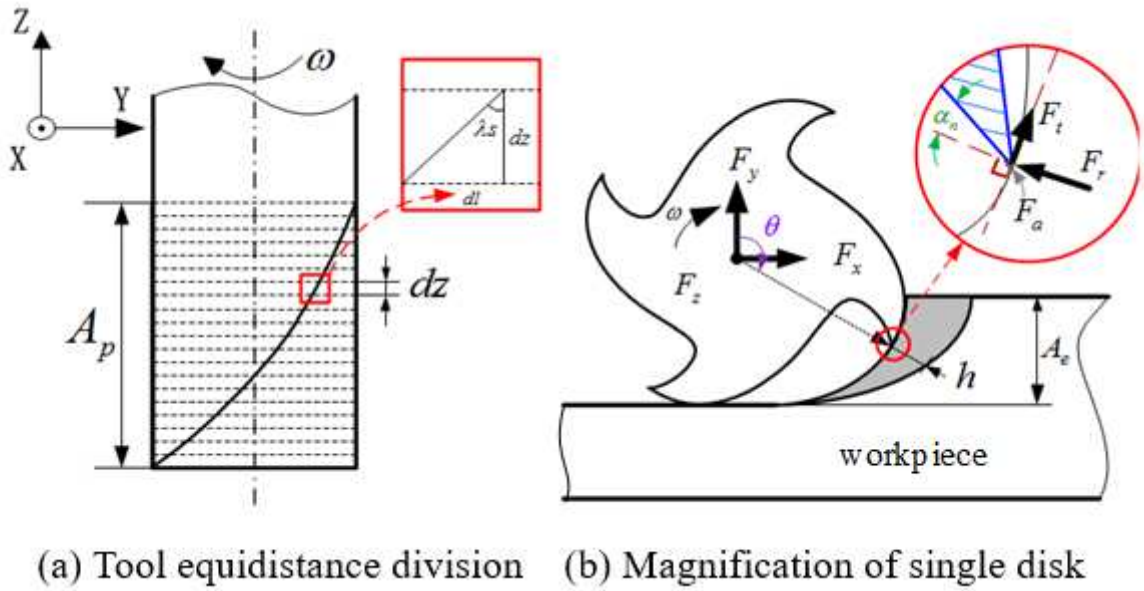

(a) Tool equidistance division (b) Magnification of single disk

Figure 2

Discretized tool along the axis

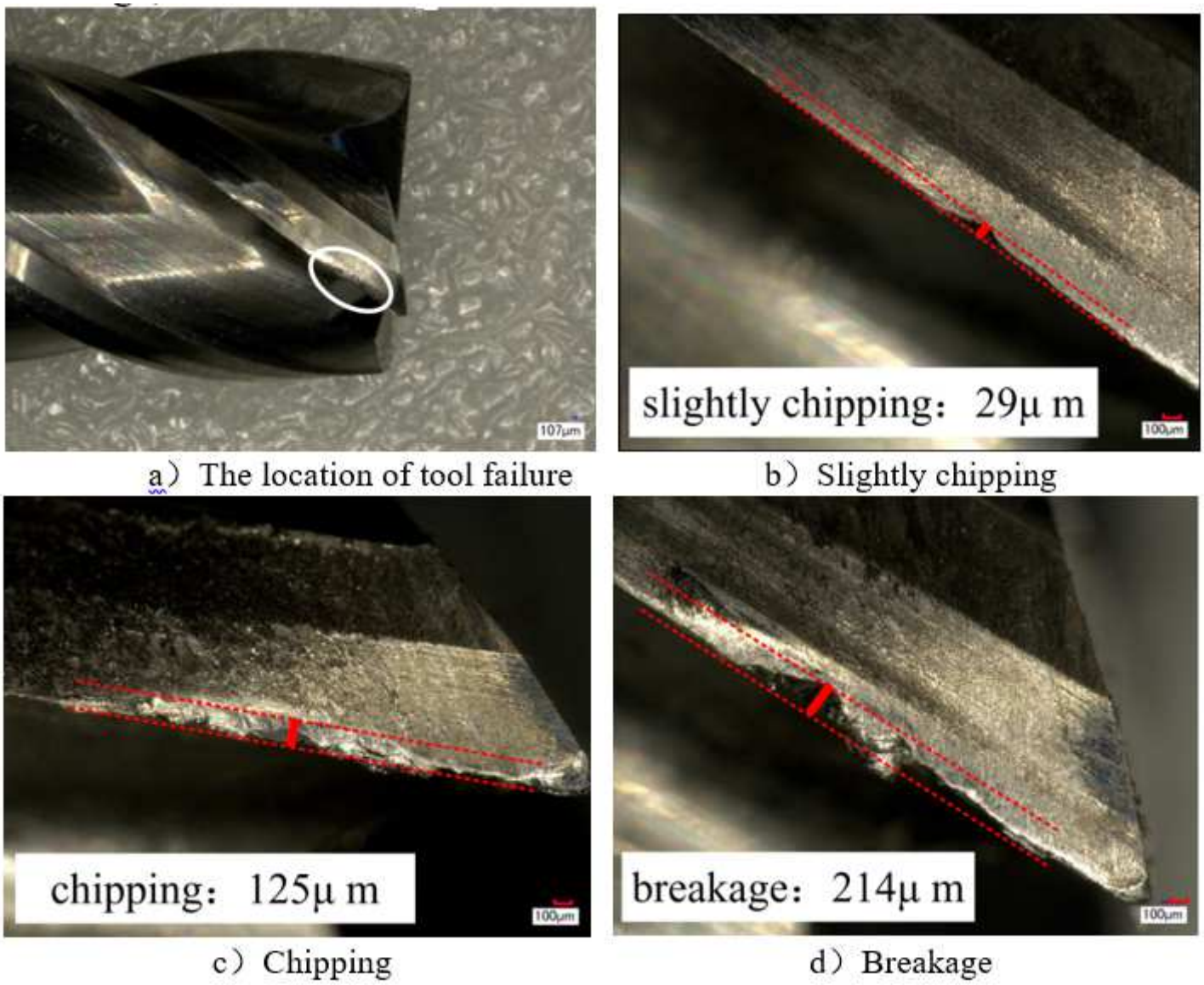

a） The location of tool failure

b） Slightly chipping

c） Chipping

d） Breakage

Figure 3

Different degree of breakage

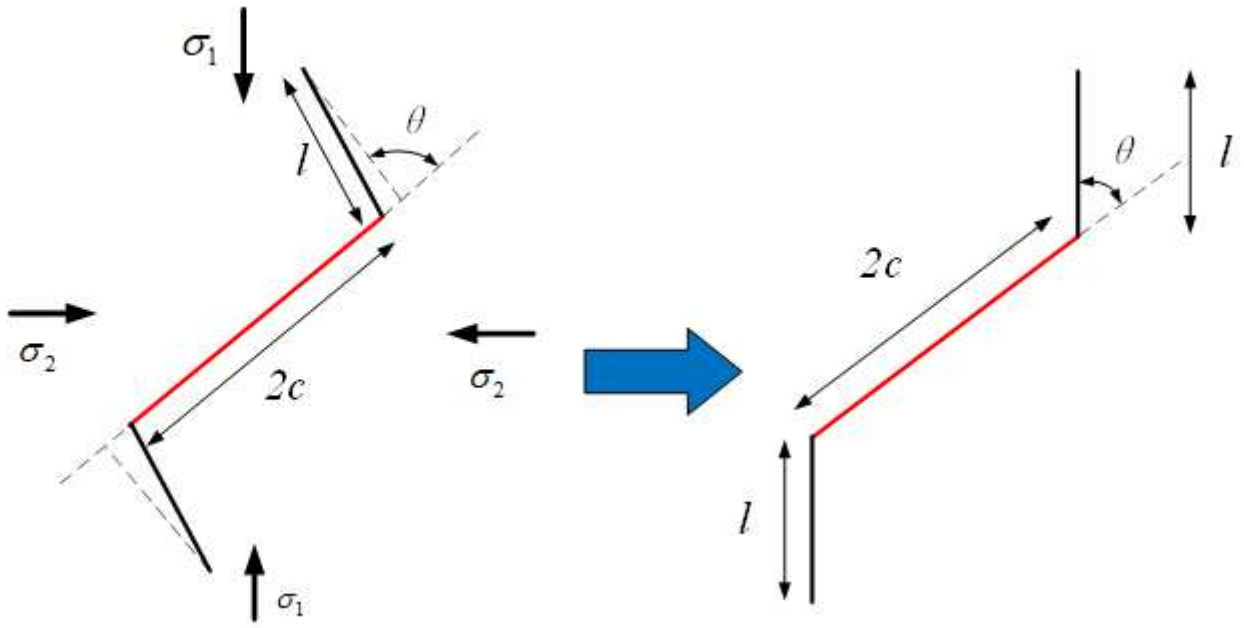

Figure 4

Slip propagation model of single crack

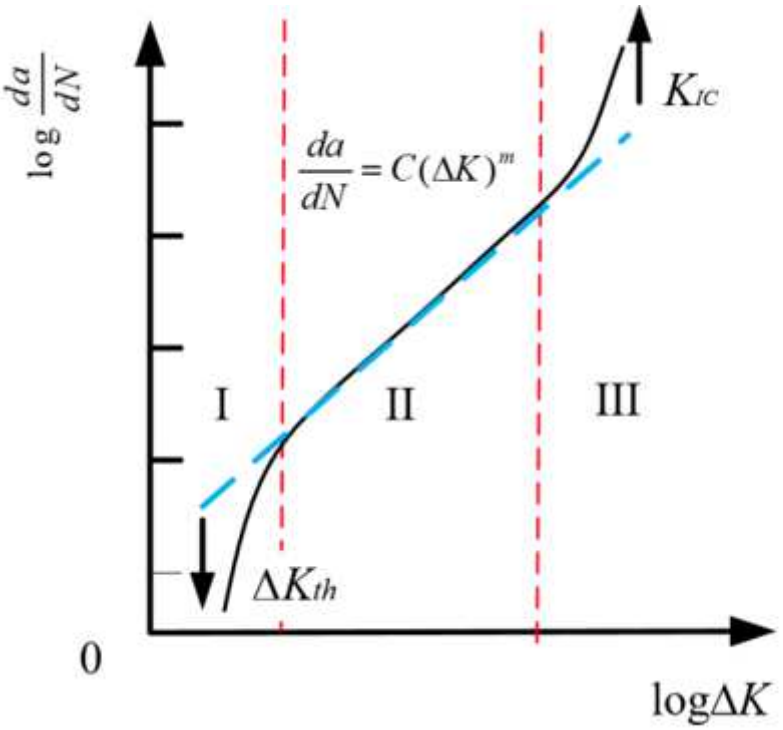

Figure 5

The relationship of dl/dn-ΔK

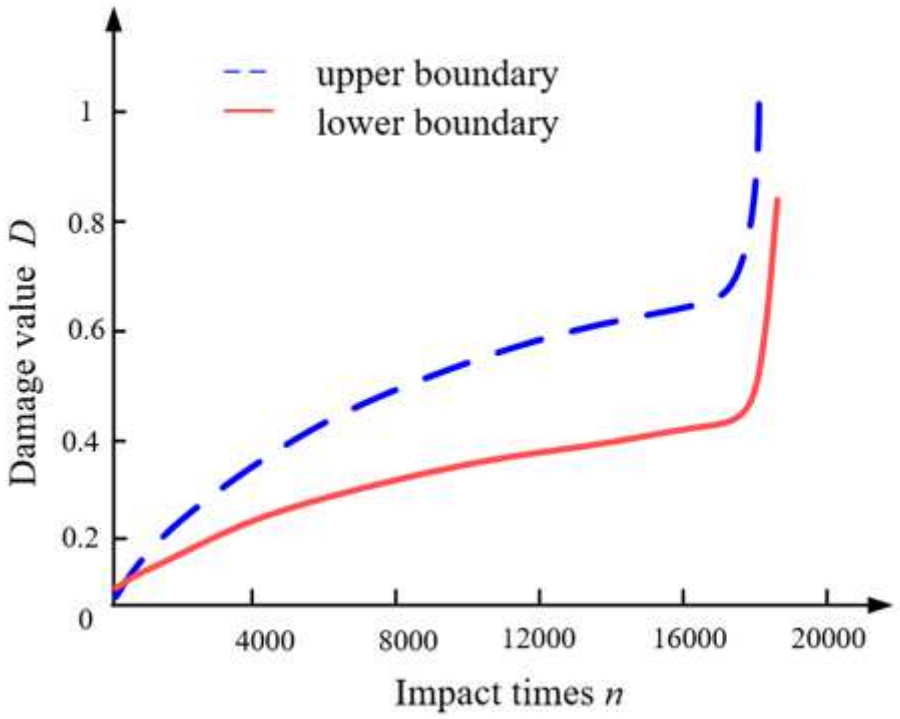

Figure 6

The damage value of tool varies with impact times

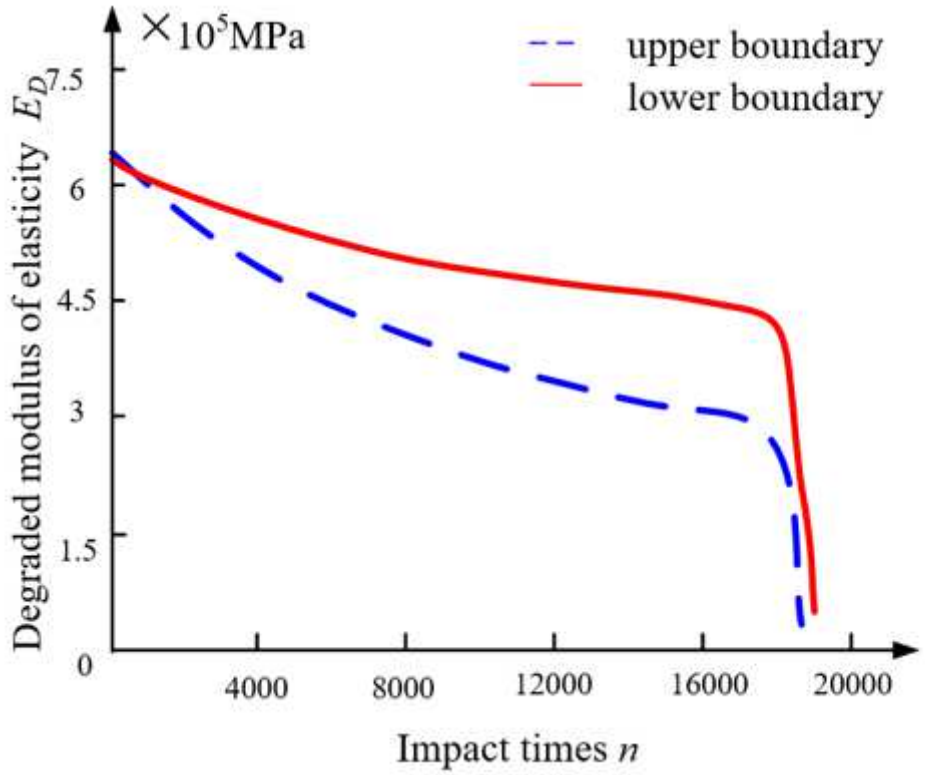

Figure 7

The elastic modulus of tool varies with impact times

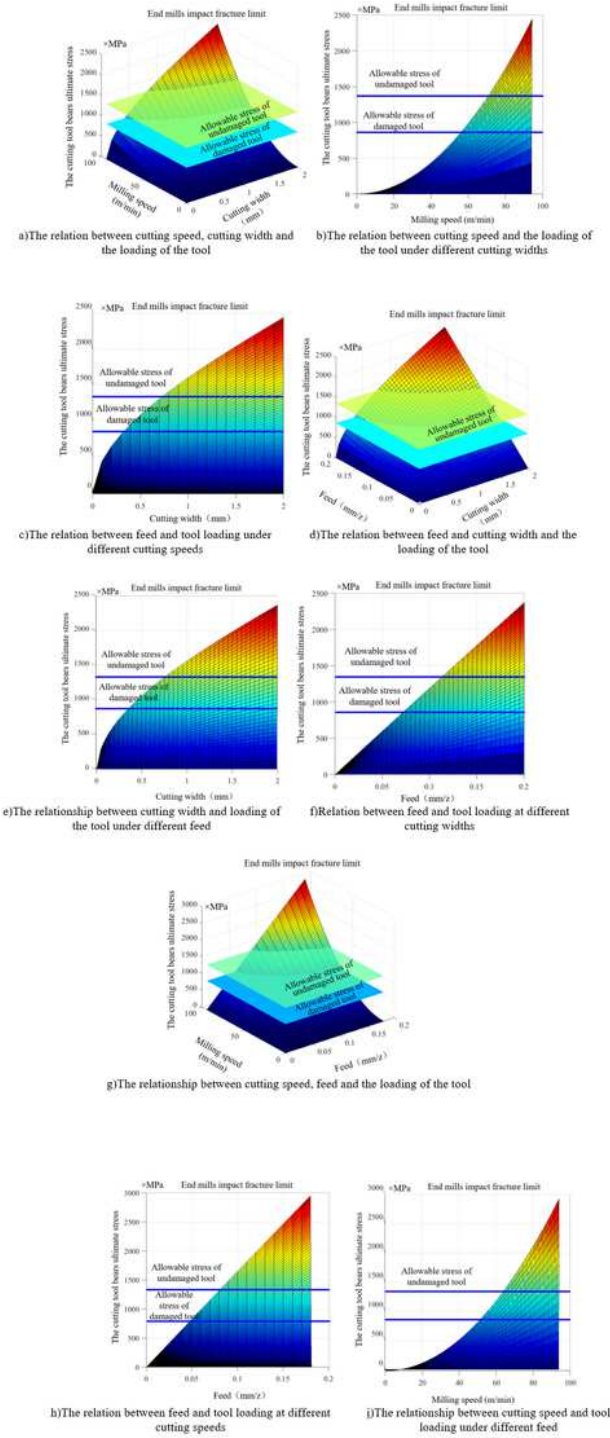

a)The relation between cutting speed, cutting width and the loading of the tool

b)The relation between cutting speed and the loading of the tool under different cutting widths

c)The relation between feed and tool loading under different cutting speeds

d)The relation between feed and cutting width and the loading of the tool

e)The relationship between cutting width and loading of the tool under different feed

f)Relation between feed and tool loading at different cutting widths

g)The relationship between cutting speed, feed and the loading of the tool

h)The relation between feed and tool loading at different cutting speeds

i)The relationship between cutting speed and tool loading under different feed

Figure 8

Diagram of feed, cutting speed, cutting depth and tool impacting on fracture loading

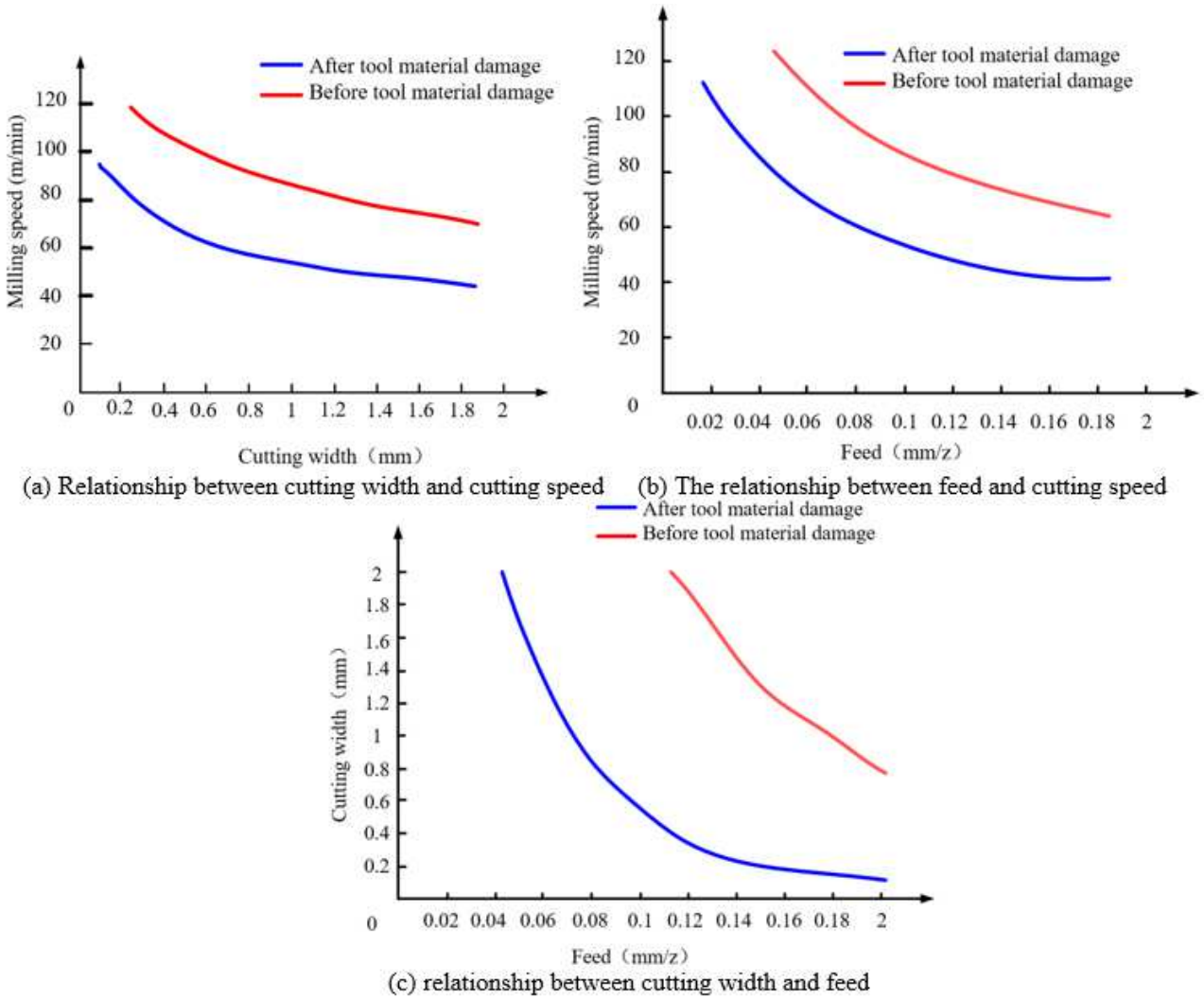

Figure 9

Safety range of milling parameters

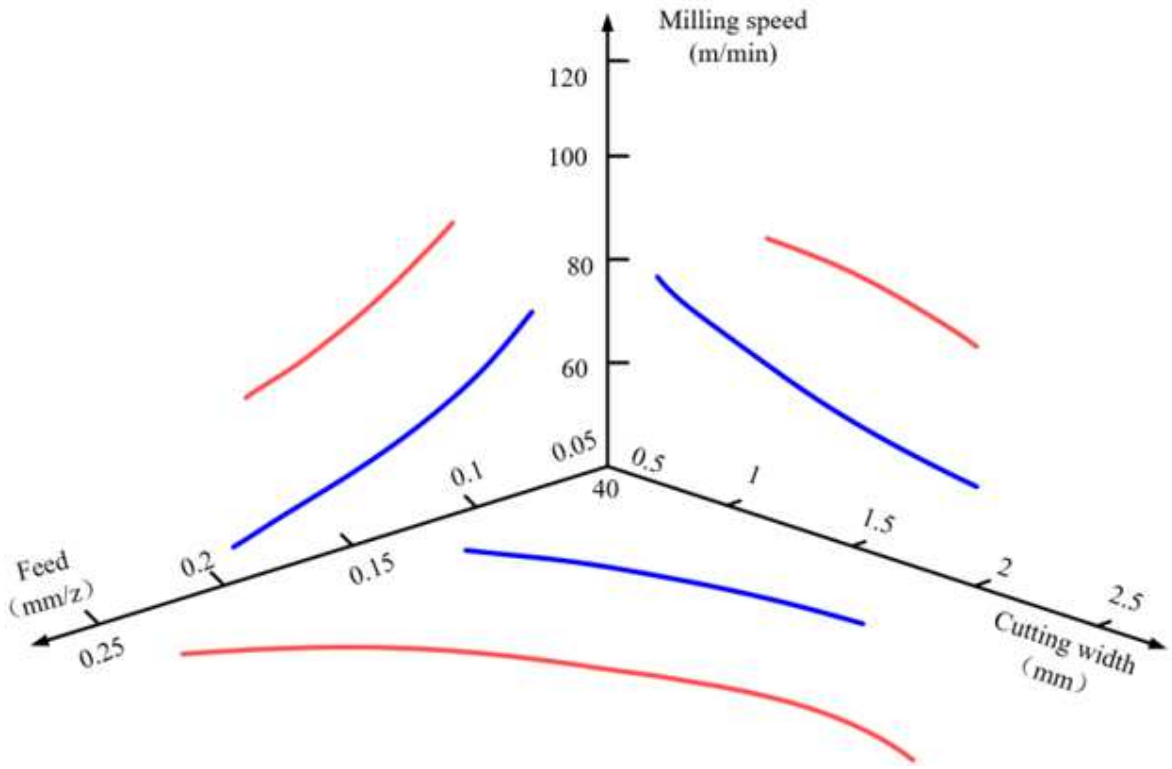

Figure 10

Safety range of milling parameters based on avoiding breakage

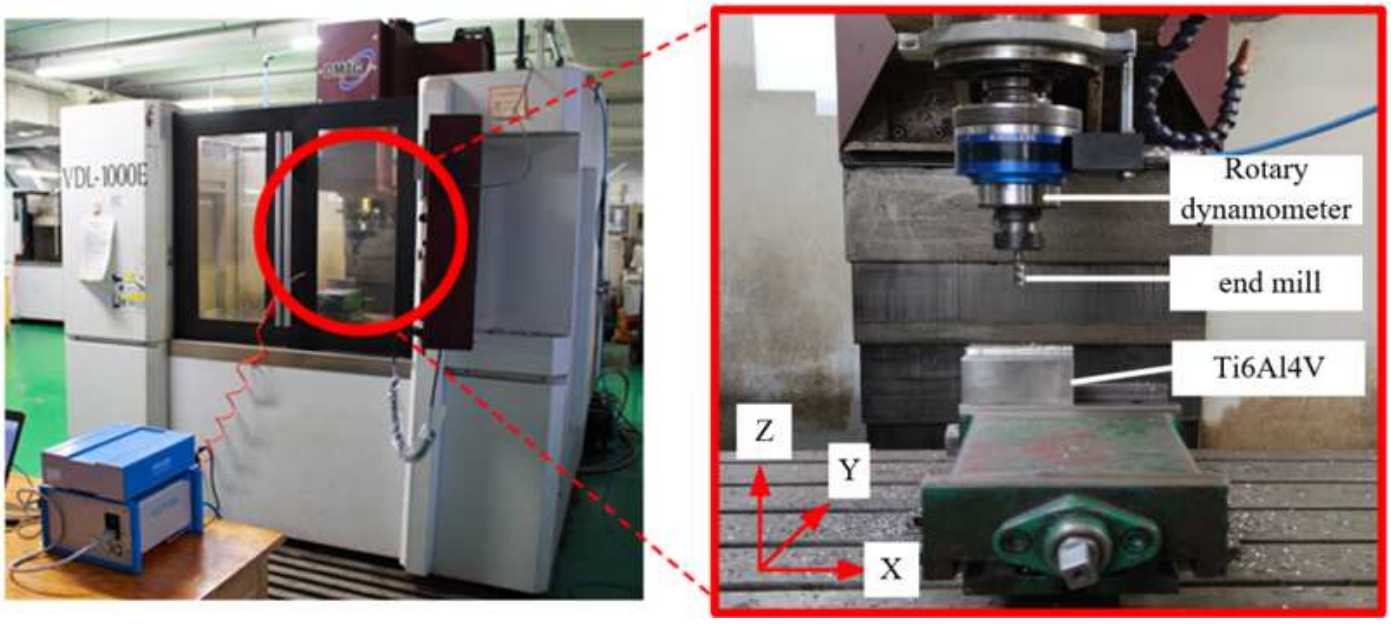

Figure 11

The test site diagram

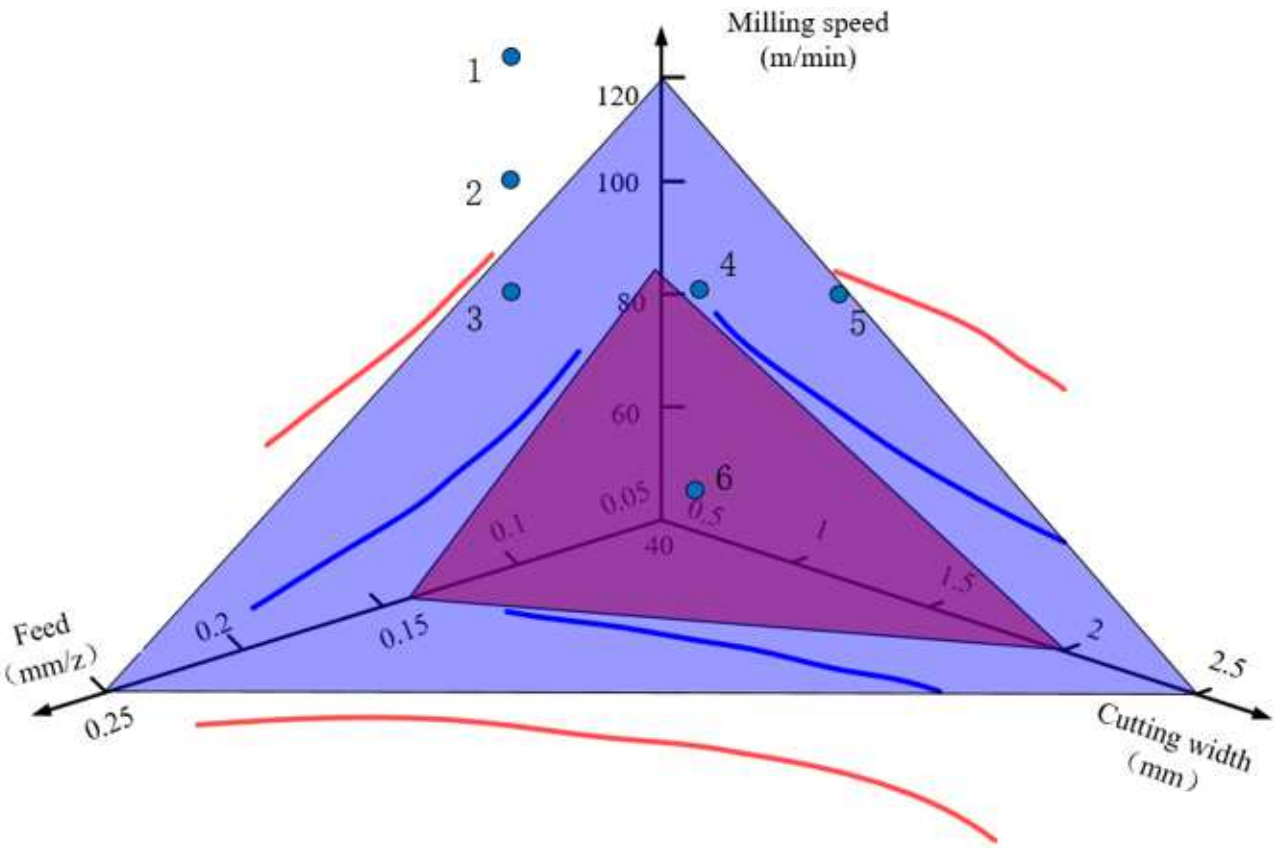

Figure 12

The optimized safety range of milling parameters based on avoiding breakage

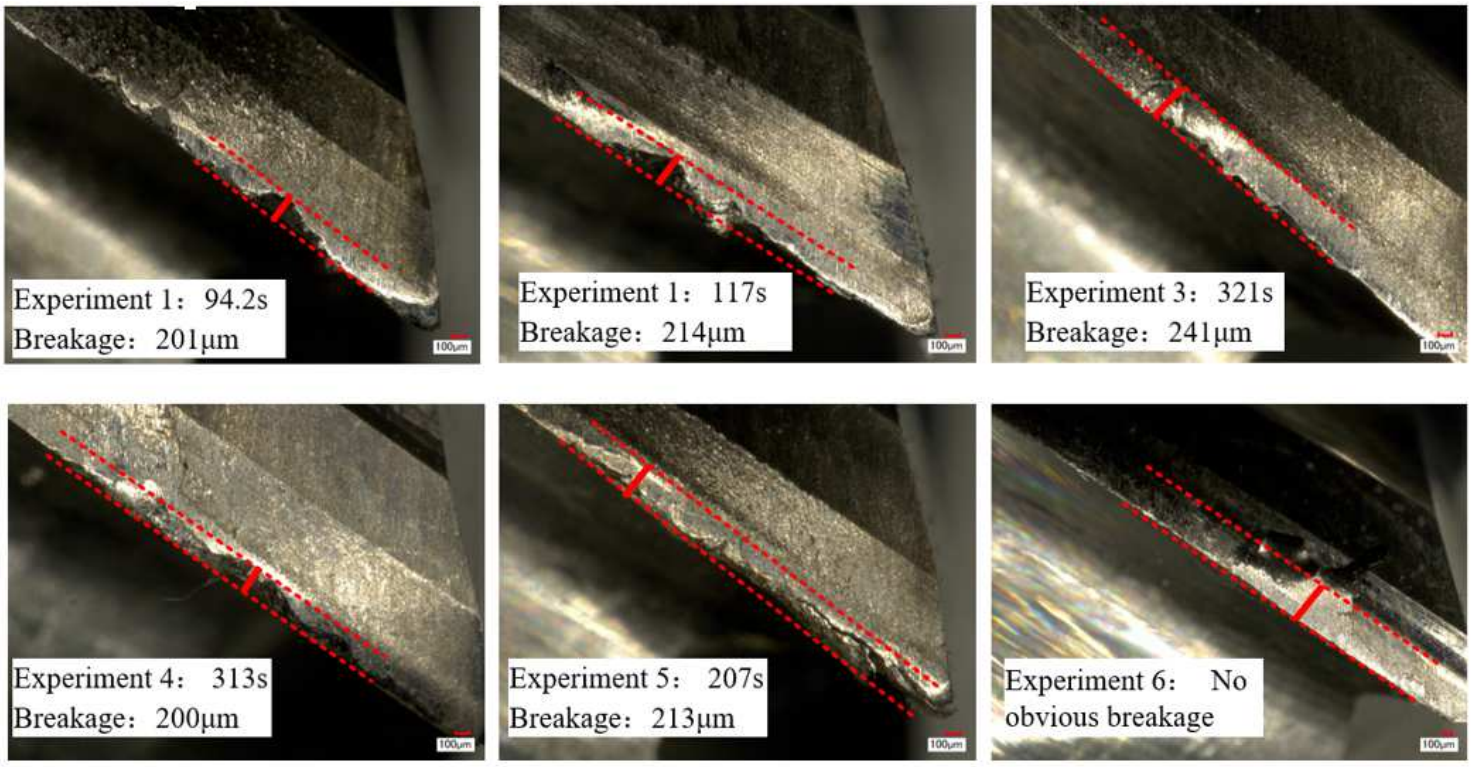

Figure 13

The result of the experiment